Journal of Inorganic Biochemistry xxx (2016) xxx–xxx

Contents lists available at ScienceDirect

Journal of Inorganic Biochemistry

journal homepage: www.elsevier.com/locate/jinorgbio

Asymmetric mono- and dinuclear Ga^{III} and Zn^{II} complexes as models for purple acid phosphatases☆

Simone Bosch [a,b], Peter Comba [a,*], Lawrence R. Gahan [b], Gerhard Schenk [b]

[a] University of Heidelberg, Institute of Inorganic Chemistry, Interdisciplinary Center for Scientific Computing, Im Neuenheimer Feld 270, D-69120 Heidelberg, Germany
[b] The University of Queensland, School of Chemistry and Molecular Biosciences, Brisbane, QLD 4072, Australia

ARTICLE INFO

Article history:
Received 27 October 2015
Received in revised form 18 December 2015
Accepted 28 December 2015
Available online xxxx

Keywords:
Phosphatase
Hydrogen bonding
Asymmetry
Dinucleating ligand
Reaction mechanism
Kinetics

ABSTRACT

Derivatives of the known dinucleating ligands HL^1 (2,6-bis{[bis(pyridin-2-ylmethyl)amino]methyl}-4-methylphenol) and H_2L^2 (2-{[bis(pyridin-2-ylmethyl)amino]methyl}-6-{[(2-hydroxybenzyl)(pyridine-2-ylmethyl)amino]methyl}-4-methylphenol) with two pivaloylamido hydrogen bond donor substituents, H_3L^3 and H_3L^5, have been prepared. The mono-, homo- and heterodinuclear Zn^{II} and Ga^{III} complexes of these ligands have been prepared and characterized. The solution equilibria are discussed on the basis of extensive NMR spectroscopic, mass spectrometric and pH-dependent UV–vis spectroscopic titrations. The phosphoester hydrolysis activity of the complexes has been studied as a function of pH and substrate concentration and analyzed using Michaelis–Menten kinetics. It emerges that the mixed metal (mixed valent) complex of the ligand with an asymmetric disposition of the hydrogen bonding substituents (H_3L^3) is a functional model for the mixed valent, dinuclear metallohydrolase purple acid phosphatase. This complex combines the essential structural features of the active site of PAP and is the first heterodinuclear model complex mimicking the essential function of PAPs, i.e. the hydrolysis of phosphomonoesters.

1. Introduction

As a prototype of dinuclear metallohydrolases, Purple Acid Phosphatases (PAPs) with two metal ions in close proximity in the active site, catalyze the hydrolysis of phosphomonoesters (Chart 1). PAPs are the only dinuclear metallohydrolases that require a mixed-valent dinuclear site (mammalian PAPs: $Fe^{III}Fe^{II}$; plant PAPs: $Fe^{III}Zn^{II}$, $Fe^{III}Mn^{II}$) [1–6]. It has been shown, however, that the replacement of the Fe^{III} center in pig PAP (ufPAP) and bovine spleen PAP (bsPAP) by a Ga^{III} ion generates $Ga^{III}Fe^{II}$ and $Ga^{III}Zn^{II}$ derivatives that exhibit activities similar to those of the native enzymes [7,8] and indicate that the diamagnetic Ga^{III} ion is able to act as a functional substitute of the paramagnetic Fe^{III} center in PAP [9].

Small heterodinuclear mixed-valent compounds, modeling the structural and functional properties of metallohydrolases, have been shown to be useful to study important features of the enzyme active sites. For example, studies with the biomimetic complex $[Fe^{III}Zn^{II}(L^2)(\mu\text{-}OAc)_2]^+$ (OAc^- = acetate; see Chart 2 for the strucure of H_2L^2 and of the other ligands discussed in this publication) have shown that (i) the model substrate BDNPP (bis-(2,4-dinitrophenyl)phosphate) only interacts with the Zn^{II} ion, and (ii) the bridging hydroxide is a much weaker nucleophile than the terminal Fe^{III}-bound hydroxide in the $[(HO)Fe^{III}(L^2)(\mu\text{-}OH)M^{II}(OH_2)]$ active species (see Chart 2 for the structure of H_2L^2 and of the other ligands discussed in this publication) [11]. The corresponding isostructural complex $[Ga^{III}Zn^{II}(L^2)(\mu\text{-}OAc)_2]^+$ exhibits a higher turnover number (TON) than the original $Fe^{III}Zn^{II}$ complex [7]. A similar result was observed from kinetic studies of the pair of complexes $[Fe^{III}Co^{II}(L^2)(\mu\text{-}OAc)_2]^+$ and $[Ga^{III}Co^{II}(L^2)(\mu\text{-}OAc)_2]^+$ [9], and Table 1 summarizes the associated known kinetic data. Similar to these biomimetic complexes, the Ga^{III} derivative of ufPAP reveals a slightly increased reactivity, consistent with the increased nucleophilicity of a Ga^{III}-bound compared to a Fe^{III}-bound hydroxide [9]. Moreover, potentiometric titrations with $[Fe^{III}Co^{II}(L^2)(\mu\text{-}OAc)_2]^+$ and $[Ga^{III}Co^{II}(L^2)(\mu\text{-}OAc)_2]^+$ support the terminal hydroxide as the acting nucleophile, as also assumed for the $[Ga^{III}Zn^{II}(L^2)(\mu\text{-}OAc)_2]^+$ and $[Fe^{III}Zn^{II}(L^2)(\mu\text{-}OAc)_2]^+$ analogs [7,9]. Kinetic studies with an $Fe^{III}Zn^{II}$ complex, anchored to 3-aminopropyl-functionalized silica (Si3AP), resulted in increased substrate affinities, compared to the unsupported catalyst [12]. This was proposed to be due to hydrogen bonds that position the substrate for the hydrolysis, similar to the proposed role of the non-coordinating histidine residues in the enzyme active sites (see Chart 1).

In the studies described here, two asymmetric and dinucleating ligands are investigated; the ligands provide two different coordination sites, mimicking the peptide backbone surrounding the dimetallic core in the active site of phosphatases. The previously reported ligand H_3L^3

☆ In memory of Professor Graeme Hanson and his contributions to Bioinorganic Chemistry and Electron Paramagnetic Resonance.

* Corresponding author.
E-mail address: peter.comba@aci.uni-heidelberg.de (P. Comba).

http://dx.doi.org/10.1016/j.jinorgbio.2015.12.028
0162-0134/

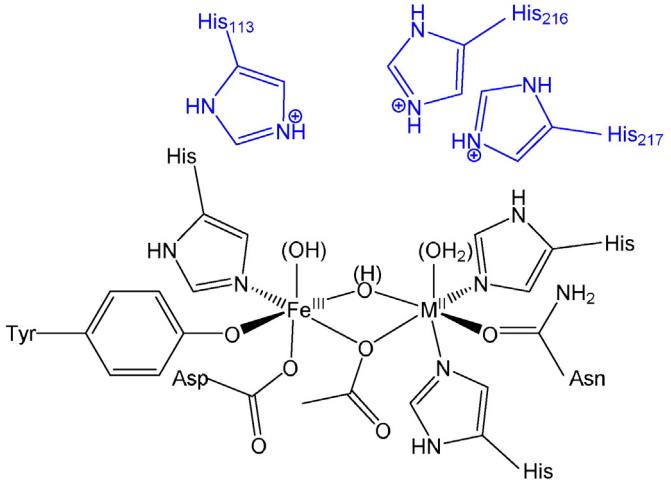

Chart 1. Schematic representation of the active site of PAP (M^{II} = Fe^{II}, Zn^{II}, Mn^{II}), including essential amino acid side chains (blue) in the second coordination sphere. [1,6,10].

is a derivative of HL^1 with the capacity to form a hydrogen-bonding network to the substrate/nucleophile in the catalytic hydrolysis of phosphoesters as present in the active site of the native enzymes. The groups capable of forming hydrogen bonds in H_3L^3 as well as H_4L^4 are two sterically demanding pivaloyl-amide residues. For ligand H_3L^3 the hydrogen bond donors are positioned asymmetrically with respect to the two coordination sites [16,17]. On the other hand the symmetric isomer H_4L^4 has one pivaloyl-amide residue at each binding site and thus combines an asymmetric primary with a symmetric secondary coordination sphere with the two different metal centers.

2. Results and discussion

2.1. Ligand synthesis

The ligand H_3L^3 was prepared as described previously [16]. The ligand H_4L^4 was obtained by reaction of 3-(chloromethyl)-2-hydroxy-5-methylbenzaldehyde (2) with *N*-(6-(((pyridin-2-ylmethyl)amino)methyl)pyridin-2-yl)pivalamide (1), followed by reaction with 2-(aminomethyl)phenol (4); subsequent amination with *N*-(6-(bromomethyl)pyridin-2-yl)pivalamide (6) yields H_4L^4 (Scheme 1).

2.2. Metal ion complexation

2.2.1. H_3L^3 with Zn^{II} and Ga^{III}

The coordination chemistry of the asymmetric ligand H_3L^3 with Zn^{II}, Cu^{II}, and Ga^{III} was examined previously using various techniques including NMR spectroscopy, single crystal X-ray diffraction, mass spectrometry, UV–vis-NIR and EPR spectroscopy, which established the selective formation of specific complexes due to the symmetry of the ligand (see Chart 3 for the proposed complex structures; these are based on observed crystal structures [16,17,18], pH-dependent titrations and NMR spectroscopy as well as mass spectra). It emerges that H_3L^3 coordinates Zn^{II} stepwise, i.e. H_3L^3 selectively yields the monozinc(II) complex in the presence of one equivalent of Zn^{II}, with the metal ion bound to binding site A (see Chart 2), prior to coordination of a second Zn^{II} ion in binding site B [16,18]. H_3L^3 achieves only the coordination of one trivalent metal ion when Ga^{III} salts are used as metal ion source. The coordination of the trivalent metal ion takes place in the sterically less congested binding site A, as shown in the X-ray structure of $[Ga^{III}(H_2L^3)(\mu\text{-}OH)]_2(ClO_4)_2$ [18]. The selectivity of the two different binding sites of the asymmetric ligand H_3L^3 is unambiguously demonstrated with the formation of a heterodinuclear $Ga^{III}Zn^{II}$ complex, independent of the order of addition of the two metal ions and even when using an excess of either of the two metal ions. The X-ray structure of $[Ga^{III}Zn^{II}(H_2L^3)(OAc)_2(\mu\text{-}OH)]_2(PF_6)_2$ confirms the results obtained by spectroscopy, i.e. that coordination of Ga^{III} occurs in the less hindered binding site A, even if this was originally occupied by Zn^{II}, and the latter finally is coordinated in the amidated binding site B [18].

2.2.2. H_4L^4–Zn^{II} chemistry

Solutions of Zn^{II} perchlorate (0.518 M, CD_3OD) were added stepwise (up to 2 equivalents) to a solution of H_4L^4 (39.5 mM, CD_3OD). After each addition, the mixture was heated for about 5 min at 50 °C, and the ^1H NMR spectrum then monitored at ambient temperature to follow the changes of the resonances of the relevant protons (see Fig. 1; ^1H NMR spectra of the entire titrations are given as Supporting Information). The formation of a monozinc(II) complex was observed upon addition of 1 equivalent Zn^{II} to a solution of H_4L^4 in methanol. Apart from the resonances assigned to the metal-free ligand, resonances of a new species appeared in mixtures with low Zn^{II} ion concentration. Finally, in the ^1H NMR spectrum obtained with a 1:1 mixture of Zn^{II} and H_4L^4, the resonances corresponding to the monozinc(II) complex of H_4L^4 were the only resonances present, i.e. no resonances attributed to the free ligand were observed. The resonances assigned to the non-amidated pyridine residues and one of the two amidated-pyridine residues exhibit shifts in the spectrum of the monozinc(II) complex of H_4L^4 compared to the metal-free ligand, while resonances assigned to the other two side-arm moieties do not show pronounced changes (Fig. 1). This suggests coordination of Zn^{II} ions in binding site C. Increasing the Zn^{II} concentration to a ratio higher than 1:1 did not lead to changes in the ^1H NMR spectrum, indicating the selective formation of the monozinc(II) complex. However, when the NMR titration experiment was conducted in acetonitrile as solvent, addition of more than one equivalent of Zn^{II} resulted in a mixture with a new species, most likely the dizinc(II) complex, in addition to the monozinc(II) complex with Zn^{II} in site C. However, complete conversion to this new species could not be observed (^1H NMR spectra of the entire titration are given as Supporting Information).

ESI^+ mass spectrometric measurements were conducted in parallel to the ^1H NMR Zn^{II} titration experiment described above, with samples taken at various steps during the ^1H NMR experiments. The mass spectrum recorded after addition of one equivalent of Zn^{II} in acetonitrile shows a main peak at m/z 806.4, associated with the monozinc(II) complex $[Zn^{II}(H_3L^4)]^+$ with the characteristic isotopic pattern for a monozinc(II) species. Further addition of Zn^{II} led to a spectrum with a 100% peak at m/z 436.7, exhibiting the isotopic pattern characteristic for a dizinc(II) species and corresponding to $[Zn^{II}_2(H_2L^4)]^{2+}$. The MS experiments support the observation from the ^1H NMR titrations of the selective formation of a monozinc(II) complex by addition of one equivalent of Zn^{II} to H_4L^4.

2.2.3. H_4L^4 - Ga^{III} and Ga^{III}/Zn^{II} chemistry

The ^1H NMR spectrum, recorded from a mixture of one equivalent of Ga^{III} perchlorate with H_4L^4 in acetonitrile (37.0 mM), and after heating for 12 h, exhibits 16 resonances in the aromatic region (Fig. 2). These resonances account for the 16 inequivalent protons of a selectively formed species. The shift of the resonances, assigned to the protons of the terminal phenol residue, indicates the coordination of the Ga^{III} ion in binding site D in the monogallium(III) complex of H_4L^4.

The mass spectrum recorded of a mixture of H_4L^4 with Ga^{III} in a ratio of 1:1 in acetonitrile shows major signals with the pattern characteristic for a monogallium(III) compound. The signals at m/z 405.7, m/z 810.3 and m/z 910.3 (besides the signal at m/z 744.4, which arises from metal-free ligand), correspond to the species $[Ga^{III}(H_3L^4)]^{2+}$, $[Ga^{III}(H_2L^4)]^+$ and $[Ga^{III}(H_2L^4)(CH_3CN)_2(OH_2)]^+$, respectively. The mass spectrometric investigation of a solution of H_4L^4 with one equivalent of Zn^{II} and one equivalent of Ga^{III} in acetonitrile, and heated for 12 h at 60 °C, resulted in a spectrum with an isotopic pattern

Please cite this article as: S. Bosch, et al., Asymmetric mono- and dinuclear GaIII and ZnII complexes as models for purple acid phosphatases, J. Inorg. Biochem. (2016), http://dx.doi.org/10.1016/j.jinorgbio.2015.12.028

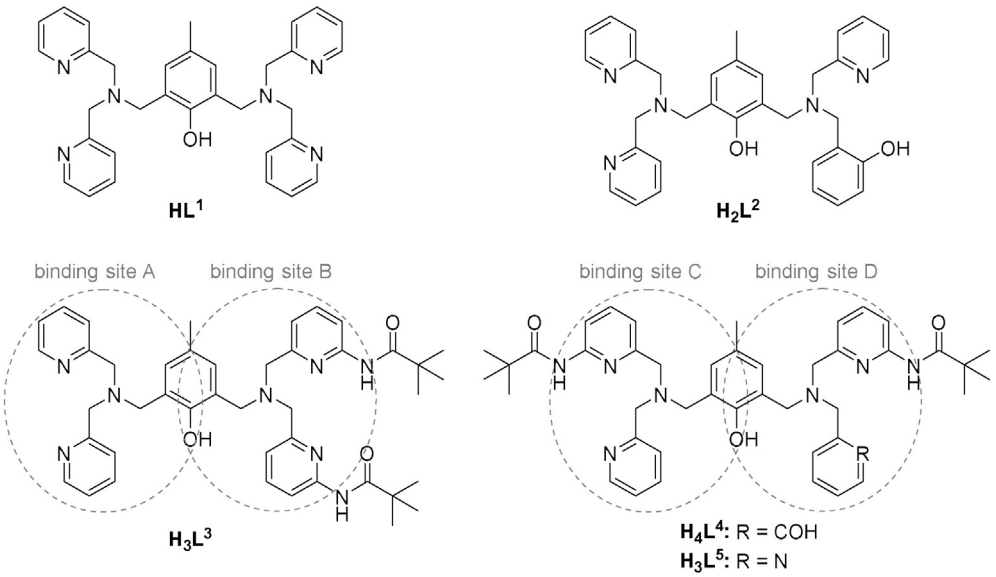

Chart 2. Ligands discussed in this work; the chart also shows the various binding sites discussed in the text.

indicative of a $Ga^{III}Zn^{II}$ species; signals associated with the remnants of the monogallium(III) complex are also present (addition of methanol was needed to obtain a well-resolved spectrum). The $Ga^{III}Zn^{II}$ complex exhibits mass to charge ratios of m/z 436.7, m/z 872.3 and m/z 972.2, matching the masses of $[Ga^{III}Zn^{II}(HL^4)]^{2+}$, $[Ga^{III}Zn^{II}(L^4)]^{+}$ and $[Ga^{III}Zn^{II}(L^4)(CH_3CN)_2(OH_2)]^{+}$, respectively.

In contrast to H_3L^3, H_4L^4 provides two chemically different binding sites with respect to the primary coordination sphere, i.e. a softer nitrogen-rich binding site C and a harder binding site D with a terminal phenolate residue. From the NMR titration and mass spectrometric experiments it emerges that, as expected, the softer Zn^{II} ion favors the softer binding site, while the harder trivalent Ga^{III} ion selectively coordinates to the harder binding site.

2.2.4. pH dependent $Ga^{III}Zn^{II}$ coordination chemistry

The ligands H_3L^3 and H_4L^4 have been shown to selectively form mononuclear Ga^{III} and Zn^{II} complexes, and they are able to generate the heterodinuclear complexes $[Ga^{III}Zn^{II}(H_2L^3)(solv)_x]^{4+}$ and $[Ga^{III}Zn^{II}(H_2L^4)(solv)_x]^{3+}$. The structural role of the two coordination sites was therefore probed by comparing the properties of the mononuclear Ga^{III} and Zn^{II} complexes with those of their heterodinuclear $Ga^{III}Zn^{II}$ derivatives as well as the dizinc(II) systems (see Chart 3).

Prior to kinetic studies (vide infra), the catalysts were prepared and characterized in solution. Separate 5 mM acetonitrile solutions of H_3L^3, H_4L^4, and the perchlorate salts of Zn^{II} and Ga^{III} were used for the sample preparations. One equivalent of ligand was treated with either (i) one equivalent of Zn^{II}, (ii) two equivalents of Zn^{II}, or (iii) one equivalent of Ga^{III}. These mixtures were then heated at 50 °C for one (Zn^{II}) or six hours (Ga^{III}), in order to completely form the complexes $[Zn^{II}(H_2L^3)(solv)_x]^{+}$, $[Zn^{II}(H_3L^4)(solv)_x]^{+}$, $[Zn^{II}_2(H_2L^3)(solv)_x]^{3+}$, $[Zn^{II}_2(H_2L^4)(solv)_x]^{2+}$, $[Ga^{III}(H_2L^3)(solv)_x]^{2+}$, and $[Ga^{III}(H_2L^4)(solv)_x]^{+}$. Solutions of $[Ga^{III}(H_2L^3)(solv)_x]^{2+}$ and $[Ga^{III}(H_2L^4)(solv)_x]^{+}$ were also treated with one equivalent of Zn^{II} and heated at 50 °C for a further one hour to generate $[Ga^{III}Zn^{II}(H_2L^3)(solv)_x]^{4+}$ and $[Ga^{III}Zn^{II}(H_2L^4)(solv)_x]^{3+}$. All final solutions were diluted with acetonitrile to obtain final complex concentrations of 1 mM.

The pK_a values of metal-bound water molecules in the various complexes were determined by spectrophotometric titrations. These titrations were carried out in acetonitrile:aqueous buffer mixtures (1:1). The aqueous buffer consisted of 2-(*N*-morpholino)ethanesulfonic acid (MES), 4-(2-hydroxyethyl)piperazine-1-ethanesulfonic acid (HEPES), 2-(cyclohexylamino)ethanesulfonic acid (CHES), 3-(cyclohexylamino)-1-propanesulfonic acid (CAPS) and lithium perchlorate for ionic strength control. The reported pH values refer to the pH of the buffer solution, and we note that the pH of an aqueous solution of the buffer is the same within error as in a 1:1 mixture of buffer and acetonitrile [14,15]. As an example, Fig. 3a shows the titration for $[Ga^{III}Zn^{II}(H_2L^3)(solv)_x]^{4+}$; the other data are given as Supporting Information. There are two isosbestic points (293 nm, 312 nm; the spectrum at pH 5.5 deviates significantly), indicating an equilibrium of two species. The absorbance vs. pH plots at different wavelengths are presented in Fig. 3b, and the fits to Eq.1, where ε_1 and ε_2 are the extinction coefficients of the protonated (HA) and deprotonated complex species (A^-) and d is the path length, result in the pK_a values listed in Table 2.

$$\text{absorbance} = (\varepsilon_1 - \varepsilon_2) * \frac{[HA]_0 * d}{10^{(pH - pK_a)} + 1} + \varepsilon_2 * [HA]_0 * d \quad (1)$$

Data fitting for $[Ga^{III}Zn^{II}(H_2L^3)(solv)_x]^{4+}$ and for $[Ga^{III}Zn^{II}(H_2L^4)(solv)_x]^{3+}$ between pH 5.5 and pH 7.5 results in a second pK_a value (these pK_a values need to be interpreted with care, as they are close to the limits of the pH range studied). Corresponding pK_a values reported for $[Ga^{III}Zn^{II}(L^2)(\mu\text{-}OAc)_2]^{+}$, p$K_a$(I) = 6.2 and p$K_a$(II) = 8.0, were assigned to the equilibria shown in Scheme 2 [7].

Comparison of the pK_a values obtained for $[Ga^{III}Zn^{II}(H_2L^4)(solv)_x]^{3+}$ and $[Ga^{III}Zn^{II}(L^2)(OAc)_2]^{+}$ indicates a shift of approximately 0.5 pH units per pivaloyl-amide residue proximal to the Ga^{III} center. An even more pronounced but similar trend was found for the monozinc(II) complexes $[Zn^{II}(H_2L^3)(solv)_x]^{+}$ and $[Zn^{II}(H_3L^4)(solv)_x]^{+}$ [18].

2.3. Phosphatase reactivity

2.3.1. Phosphoester hydrolysis

The influence of hydrogen bonding on the phosphoester hydrolysis reactivity was probed with a well-established spectrophotometric assay, using BDNPP as substrate [19]. Cleavage of the phosphorous–oxygen bond was followed at 25 °C by monitoring the hydrolysis product 2,4-dinitrophenolate by its strong absorption at 400 nm (ε = 12,100 $M^{-1}\,cm^{-1}$) [19]. All measurements were carried out in 1:1 acetonitrile–buffer mixtures. The pH dependence of the activity was studied in the pH range of 5 to 11 by varying the pH of the multicomponent buffer (Figs. 4 and 5; the pH values refer to the aqueous component). The

Table 1
Kinetic data (k_{cat} in [10^{-3} s^{-1}], K_M in [mM] and k_{cat}/K_M in [s^{-1} M^{-1}]) of BDNPP hydrolysis (all kinetic studies were done in a mixture of acetonitrile:aqueous buffer = 1:1)[a].

Complex	pK_a(I)[b]	pK_a(II)[b]	k_{cat}	K_M	k_{cat}/K_M	pH[c]
$[Fe^{III}Zn^{II}(L^2)(\mu\text{-}OAc)_2]^+$ [13]	4.8	7.5	0.73	8.10	0.09	6.1
$[Fe^{III}Zn^{II}(L^2)(\mu\text{-}OH)_2]^+$ [11]	5.3	8.1	0.91	4.20	0.22	6.5
$[Ga^{III}Zn^{II}(L^2)(\mu\text{-}OAc)_2]^+$ [7]	5.4	8.6	1.41	7.15	0.20	6.8
$[Fe^{III}Co^{II}(L^2)(\mu\text{-}OAc)_2]^+$ [9]	5.2	8.8	1.42	92.7	0.02	7.0
$[Ga^{III}Co^{II}(L^2)(\mu\text{-}OAc)_2]^+$ [9]	5.7	8.9	1.87	88.1	0.02	7.5
$[Fe^{III}Zn^{II}(HL^6)(\mu\text{-}OH)(H_2O)]^{2+}$ [d] [12]	–	–	0.90	3.55	0.25	7.0
$[Fe^{III}Zn^{II}(Si3AP\text{-}L^6)(\mu\text{-}OH)(H_2O)]^{2+}$ [d] [12]	–	–	0.14	1.54	0.09	7.0

[a] The pH values refer to the aqueous component; the pH of a 1:1 mixture of buffer and acetonitrile is the same within the error as in an aqueous solution of the buffer [14,15].
[b] The pK_a values refer to coordinated H_2O molecules after dissociation of OAc in aqueous solution, see Scheme 2 below and corresponding text.
[c] pH of aqueous buffer solution used for substrate dependence assays (Michaelis–Menten measurements).
[d] H_2L^6 = 3-(((3-((bis(pyridin-2-ylmethyl)amino)methyl)-2-hydroxy-5-methylbenzyl)(pyridin-2-ylmethyl)amino)methyl)-2-hydroxy-5-methylbenzaldehyde.

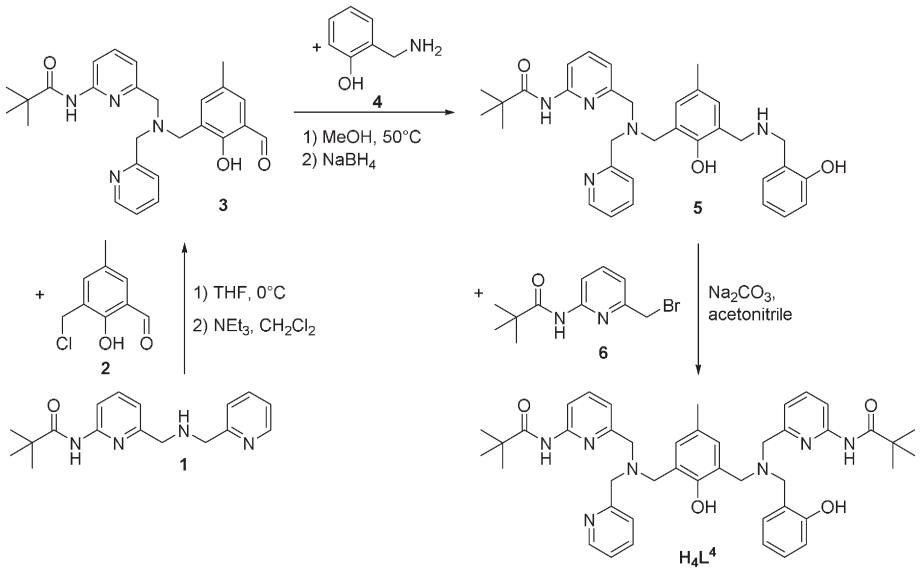

Scheme 1. Synthesis of H_4L^4.

resulting data were fitted to Eq.2, which is based on a model for a diprotic system with two active species [20].

$$v_0 = \frac{v_{max}\left(1+\frac{\gamma K_{a2}}{[H^+]}\right)}{\left(1+\frac{[H^+]}{K_{a1}}+\frac{K_{a2}}{[H^+]}\right)} \quad (2)$$

Here, v_0 is the initial and v_{max} the maximum reaction rate that is reached under given conditions. The factor γ is related to the relative activity of the two active species in equilibrium (E^nS and $E^{n-1}S$); a value of γ less than unity corresponds to a more active E^nS adduct and a value higher than one considers the deprotonated adduct $E^{n-1}S$ as more active [20,21]. The K_a values obtained are the protonation equilibrium constants between the two relevant active species. The resulting pK_a and γ values are listed in Table 3 – note that it is not unexpected that the pK_a values emerging from potentiometric titrations and kinetics are somewhat different; among others this is due to the presence of the substrate in the kinetic experiments. Phosphatase activity studies were undertaken with the two heterodinuclear $Ga^{III}Zn^{II}$ complexes of H_3L^3 and H_4L^4 as well as their monogallium(III), monozinc(II), and dizinc(II) complexes (see Section 4 for details).

2.3.2. pH dependent kinetics

The examination of BDNPP hydrolysis by the mono- and dinuclear complexes of H_3L^3 reveals different pH dependences. The monozinc(II) complex, $[Zn^{II}(H_2L^3)(solv)_x]^+$, with Zn^{II} in the amide-free binding site A, is only active under basic conditions and shows very little activity below pH 7.5. Since deprotonation of the coordinated H_2O of $[Zn^{II}(H_2L^3)(solv)_x]^+$ is close to the limit of the accessible pH range, the fitted pK_a and γ values need to be interpreted with care. The dizinc(II) complex of HL^1 with two Zn^{II} centers in coordination spheres similar to that of $[Zn^{II}(H_2L^3)(solv)_x]^+$ but without a hydrogen bonding network, has pK_a values of 6.5 and 10.3 and shows hydrolysis activity in the pH range between these two pK_a values [16]. Therefore, the lack of activity of $[Zn^{II}(H_2L^3)(solv)_x]^+$ at pH < 7.5 seems to be due to the inability of cooperative interaction between two Zn^{II} centers. The pH dependence of $[Zn^{II}_2(H_2L^3)(solv)_x]^{3+}$, with both coordination sites occupied by Zn^{II} supports this assumption, as it exhibits BDNPP hydrolysis activity below pH 7.5.

In contrast to the mono- and dizinc(II) complexes of H_3L^3, the monogallium(III) complex $[Ga^{III}(H_2L^3)(solv)_x]^+$ shows a bell-shaped profile in the v_0 vs. pH plot. This complex is only catalytically active in the pH range between the two pK_a values of 6.3 and 8.6, indicating that the active species is $[Ga^{III}(H_2L^3)(OH)(OH_2)]$. Protonation and deprotonation of the catalytically competent complex lead to a strong decrease of activity. When the second coordination site of the monogallium(III) complex is coordinated to Zn^{II}, a superposition of the profiles found for $[Zn^{II}(H_2L^3)(solv)_x]^+$ and $[Ga^{III}(H_2L^3)(solv)_x]^{2+}$ is observed, but the initial rate at pH 7 is higher than the sum of the corresponding initial rates of the monocomplexes, indicating again cooperativity.

Comparison of the hydrolysis activity of the two mononuclear complexes of H_3L^3 provides insight into the catalytic role of the metal ion. While $[Zn^{II}(H_2L^3)(solv)_x]^+$ is only active at high pH, $[Ga^{III}(H_2L^3)$

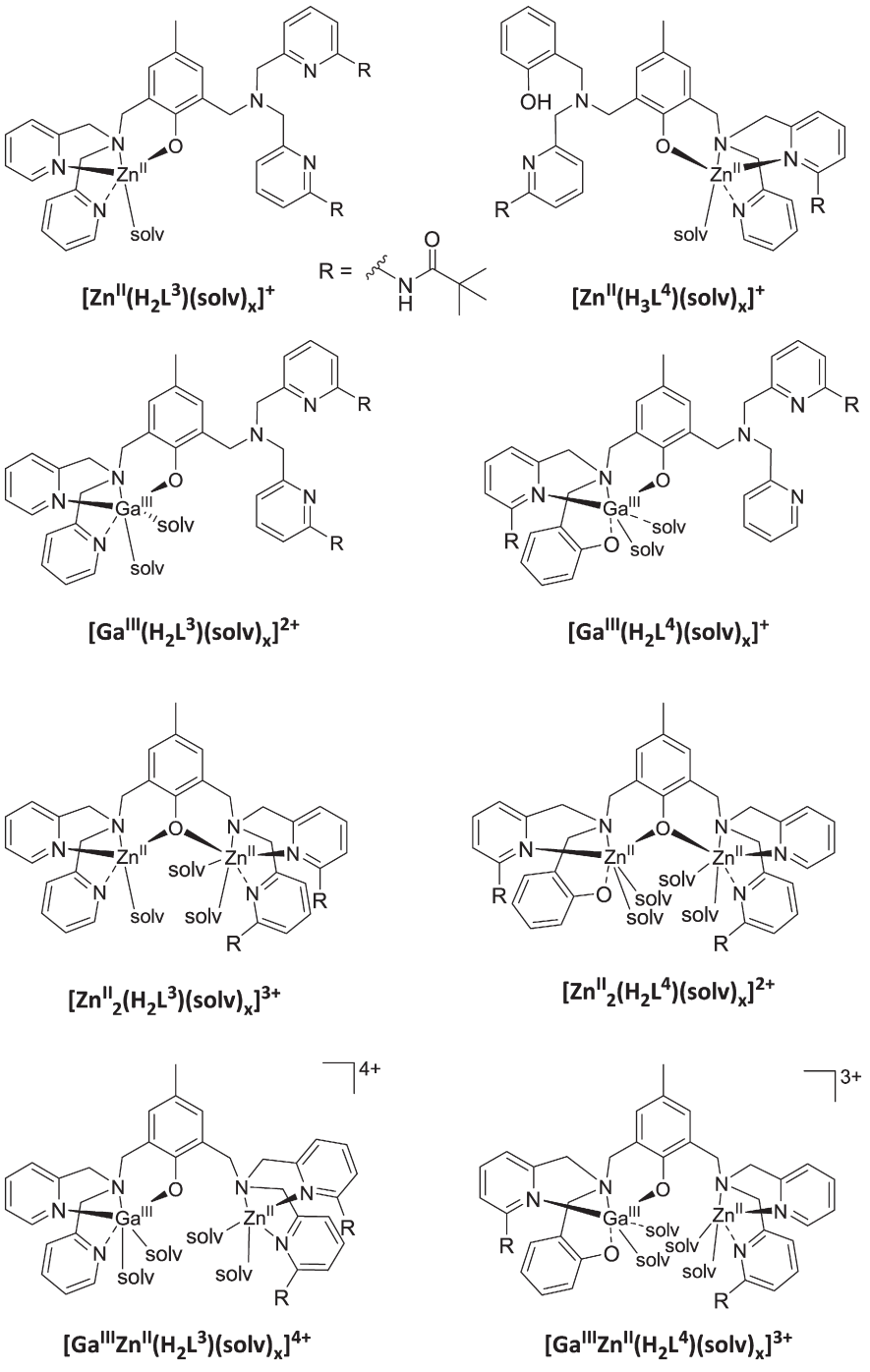

Chart 3. Complexes discussed in this manuscript.

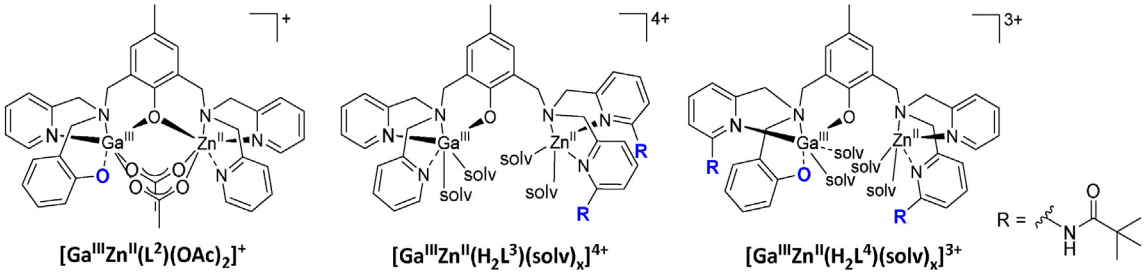

Chart 4. $Ga^{III}Zn^{II}$ complexes discussed.

Please cite this article as: S. Bosch, et al., Asymmetric mono- and dinuclear GaIII and ZnII complexes as models for purple acid phosphatases, J. Inorg. Biochem. (2016), http://dx.doi.org/10.1016/j.jinorgbio.2015.12.028

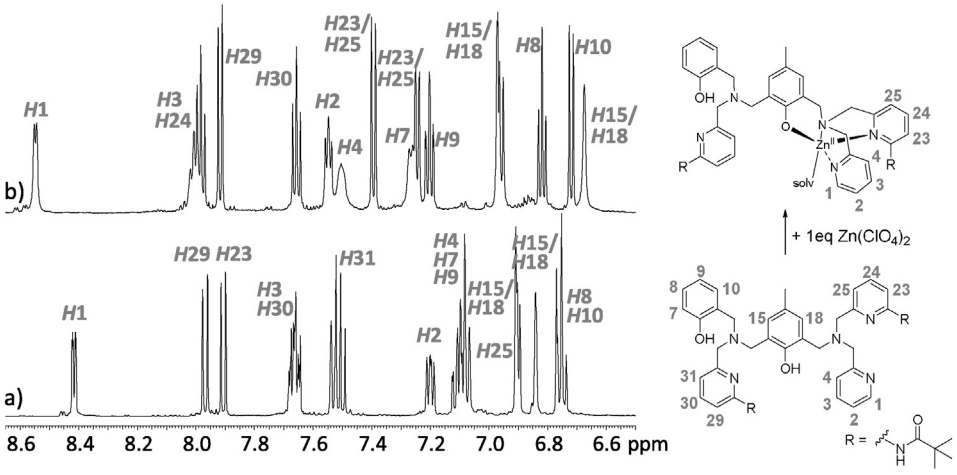

Fig. 1. Comparison of the aromatic regions in the ^{1}H NMR spectra of a)H_4L^4 with b) 1.0 eq. of $Zn^{II}(ClO_4)_2$ in CD_3OD.

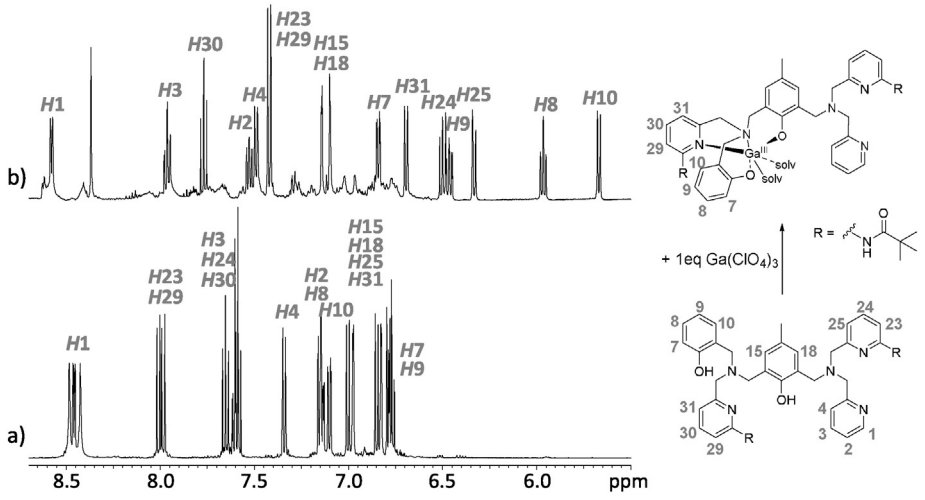

Fig. 2. Comparison of the aromatic regions in the ^{1}H NMR spectra of a) H_4L^4 with b) 1.0: eq of $Ga^{III}(ClO_4)_3$ in CD_3CN heated at 60 °C for 12 h.

$(solv)_x]^+$ is active at low pH, indicating that with a Zn^{II} active site, a high enough concentration of hydroxide is essential to ensure phosphoester hydrolysis. The fact that the metal-free ligand, as well as ligand-free Zn^{II}, are not catalytically active over the entire pH range illustrates the requirement for Zn^{II} to be coordinated to the ligand for activation and hydrolysis of the phosphoester substrate. With $[Ga^{III}(H_2L^3)(solv)_x]^+$, the hydrolysis observed at low pH is due to the strong Lewis acidity of Ga^{III}, which is able to provide the nucleophile for phosphoester hydrolysis at near neutral pH. Ga^{III} ions in absence of ligand are not able to hydrolyze BDNPP. The fact that with $[Ga^{III}(H_2L^3)(solv)_x]^+$ at high pH only autohydrolysis is observed indicates that the Ga^{III} complex in the doubly deprotonated species, most likely $[Ga^{III}(H_2L^3)(OH)_2]$, is not able to activate the phosphoester substrate.

Table 2
pK_a values determined by spectrophotometric titration.

Complex	pK_a	Complex	pK_a
$[Zn^{II}(H_2L^3)(solv)_x]^+$	7.3 ± 0.2	$[Zn^{II}(H_3L^4)(solv)_x]$	8.4 ± 0.5
$[Zn^{II}_2(H_2L^3)(solv)_x]^{3+}$	6.9 ± 0.6	$[Zn^{II}_2(H_2L^4)(solv)_x]^{2+}$	9.8 ± 0.1
$[Ga^{III}(H_2L^3)(solv)_x]^{2+}$	6.7 ± 0.9 9.1 ± 0.4	$[Ga^{III}(H_2L^4)(solv)_x]^+$	7.1 ± 0.7
$[Ga^{III}Zn^{II}(H_2L^3)(solv)_x]^{4+}$	(5.9 ± 0.4)[a] 8.4 ± 0.2	$[Ga^{III}Zn^{II}(H_2L^4)(solv)_x]^{3+}$	6.7 ± 0.4 (10.6 ± 0.1)[a]

[a] Determined pK_a values are close to the limit of the examined pH range.

The pH dependence experiments of BDNPP hydrolysis for the H_3L^4 based systems lead to similar interpretations (see Fig. 5), i.e. (i) $[Zn^{II}(H_3L^4)(solv)_x]^+$ is only active under strongly basic conditions, (ii) $[Ga^{III}(H_2L^4)(solv)_x]^+$ is active in a defined pH region between two relevant pK_a values (6.74 and 8.68), and (iii) $[Ga^{III}Zn^{II}(H_2L^4)(solv)_x]^{3+}$ exhibits a superposition of the behavior found for $[Zn^{II}(H_3L^4)(solv)_x]^+$ and $[Ga^{III}(H_2L^4)(solv)_x]^+$.

2.3.3. Substrate concentration dependent kinetics

The substrate concentration dependence was probed for the mono- and heterodinuclear complexes of H_3L^3 and H_4L^4 at pH 7 (0.5 mM < $[BDNPP]_0$ < 4.14 mM). Saturation behavior was achieved for all systems except for $[Ga^{III}(H_2L^3)(solv)_x]^+$. The resulting values of k_{cat} and K_M are listed in Table 3. The catalytic efficiencies k_{cat}/K_M have also been determined but the corresponding standard deviations preclude a meaningful interpretation (a Table with k_{cat}/K_M included appears as Supporting Information).

A vacant coordination site in a potentially dinuclear system was shown to be able to accelerate phosphoester hydrolysis [22,23]. This is not observed for our phenolate-based complexes, since the Zn^{II}_2 complexes of HL^1 and H_3L^3 exhibit much higher hydrolysis rates than

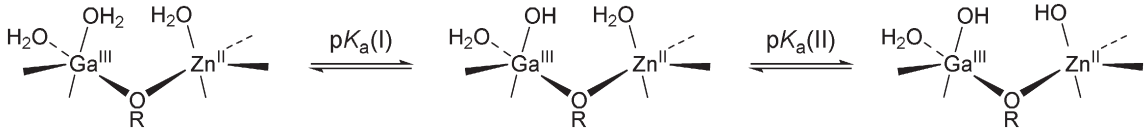

Scheme 2. Illustration of the protonation equilibria for $Ga^{III}Zn^{II}$ complexes present in basic solution (OR = bridging phenolate of the ligand backbone) [7].

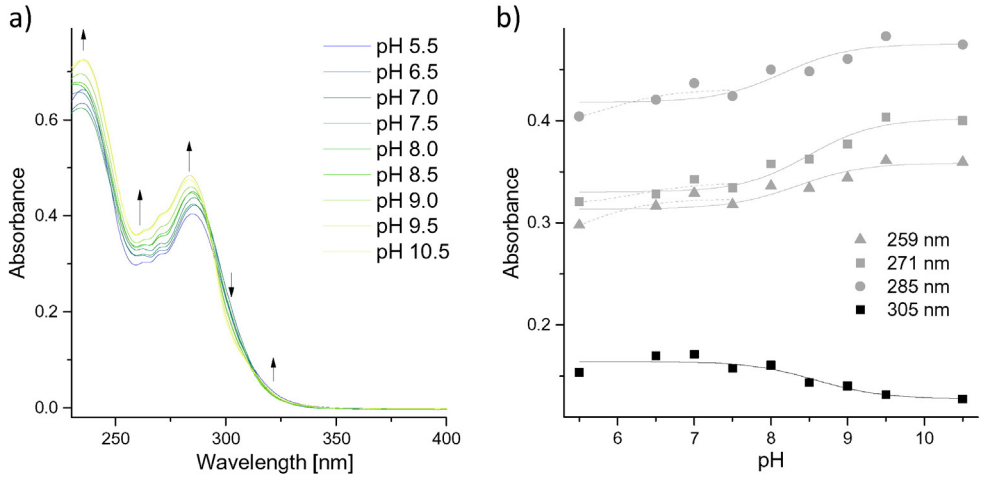

Fig. 3. a) Spectrophotometric titration (25 μM in acetonitrile:aqueous buffer between pH 5.5 and 10.5); b) absorbance vs. pH plot for $[Ga^{III}Zn^{II}(H_2L^3)(solv)_x]^{4+}$.

$[Zn^{II}(H_2L^3)(solv)_x]^+$. The K_M values of $[Zn^{II}(H_2L^3)(solv)_x]^+$ (K_M = 4 mM) and $[Zn^{II}_2(H_2L^3)(\mu\text{-OAc})(OH)]^+$ (K_M = 4 mM) are much lower than those of $[Zn^{II}_2(L^1)(\mu\text{-OAc})_2]^+$ (K_M = 123 mM) [16], indicating a significant enhancement on the substrate affinity by the hydrogen bonding network. The substrate concentration dependences indicate that the exchange of Zn^{II} in binding site A ($[Zn^{II}(H_2L^3)(solv)_x]^+$) by Ga^{III}, and subsequent coordination of Zn^{II} to site B to produce $[Ga^{III}Zn^{II}(H_2L^3)(solv)_x]^{4+}$, leads to a 54-fold increase in the phosphoester hydrolysis rate but the value for K_M also rises, i.e. the substrate affinity decreases. However, the catalytic efficiency of $[Ga^{III}Zn^{II}(H_2L^3)(solv)_x]^{4+}$ is still significantly higher than that of $[Zn^{II}(H_2L^3)(solv)_x]^+$ (see Supporting Information). Comparison of the kinetic parameters for the $Ga^{III}Zn^{II}$ complex of H_3L^3 with those obtained for $[Zn^{II}_2(H_2L^3)(\mu\text{-OAc})(OH)]^+$ (k_{cat} = (0.57 ± 0.04)·10^{-3} s^{-1}; K_M = (4 ± 1) mM; k_{cat}/K_M = 0.14 s^{-1} M^{-1}; [16] reveals that the heterodinuclear $Ga^{III}Zn^{II}$ complex hydrolyzes BDNPP about twenty times faster at neutral pH. Although the substrate affinity of the $Ga^{III}Zn^{II}$ complex is significantly lower, the catalytic efficiency of $[Ga^{III}Zn^{II}(H_2L^3)(solv)_x]^{4+}$ is increased significantly compared to the Zn^{II}_2 system (see Supporting Information), illustrating the importance of the trivalent metal ion.

The substrate concentration dependence measurements of the H_3L^4 based systems reveal that the hydrolysis rate of the $Ga^{III}Zn^{II}$ complex is increased threefold compared to the monogallium(III) complex and increased 15-fold compared to the monozinc(II) complex. However, the substrate affinity of the $Ga^{III}Zn^{II}$ complex is similar to that of the Ga^{III} complex and significantly lower than that of the Zn^{II} complex. In contrast to the corresponding complexes of H_3L^3, $[Zn^{II}(H_3L^4)(solv)_x]^+$ has the Zn^{II} cation in the same binding site as $[Ga^{III}Zn^{II}(H_2L^4)(solv)_x]^{3+}$ and $[Ga^{III}(H_2L^4)(solv)_x]^+$ has Ga^{III} in the same binding site as $[Ga^{III}Zn^{II}(H_2L^4)(solv)_x]^{3+}$. Therefore, the fact that the $Ga^{III}Zn^{II}$ complex of H_4L^4 exhibits a faster hydrolysis rate than the sum of the rates of the monozinc(II) and monogallium(III) complexes can be attributed to cooperativity between the two metal ions.

Independent of the ligand backbone (H_3L^3 vs. H_4L^4), complexes with the same metal ions coordinated show similar pH dependences of the

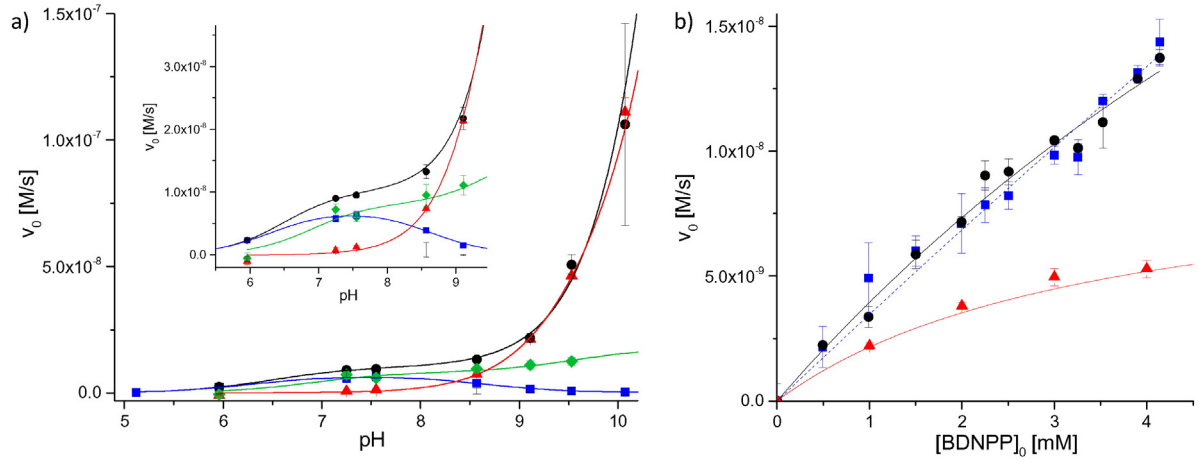

Fig. 4. a) pH dependence (0.04 mM in complex, 5 mM in BDNPP) and b) substrate concentration dependence at pH = 7 (0.04 mM in complex) of the BDNPP hydrolysis activity for mixtures of H_3L^3 with 1 eq Zn^{II} (red triangles), 2 eq Zn^{II} (green diamonds), 1 eq Ga^{III} (blue squares), or 1 eq Ga^{III} followed by 1 eq Zn^{II} (black circles).

Please cite this article as: S. Bosch, et al., Asymmetric mono- and dinuclear GaIII and ZnII complexes as models for purple acid phosphatases, J. Inorg. Biochem. (2016), http://dx.doi.org/10.1016/j.jinorgbio.2015.12.028

Table 3
Kinetic data (k_{cat} in [10^{-3} s^{-1}] and K_M in [mM] of BDNPP hydrolysis with mixtures of the ligands H_3L^3 or H_4L^4 with 1 eq Zn^{II}, 2 eq Zn^{II}, 1 eq Ga^{III}, or 1 eq Ga^{III} followed by 1 eq Zn^{II} (all kinetics in a mixture of acetonitrile–aqueous buffer solution (1:1)).

Complex	pK_a(I)	pK_a(II)	γ	k_{cat}[a]	K_M[a]
$[Zn^{II}_2(L^1)(OAc)_2]^+$ [20]	6.5	10.3	1.26 ± 0.08	7.18 ± 4.39	123 ± 79
$[Zn^{II}(H_2L^3)(solv)_x]^+$	9.2 ± 0.5 [c]	10.9 ± 0.5 [c]	14.94 ± 7.00 [c]	0.24 ± 0.02	4 ± 1
$[Zn^{II}_2(H_2L^3)(solv)_x]^{3+}$	6.9 ± 0.4	9.6 ± 0.3	2.21 ± 0.64	n.a.	n.a.
$[Zn^{II}_2(H_2L^3)(OAc)(OH)]^+$ [16]	7.0	10.7	0.45 ± 0.14	0.57 ± 0.04	4 ± 1
$[Ga^{III}(H_2L^3)(solv)_x]^{2+}$	6.3 ± 0.2	8.6 ± 0.2	0.01 ± 0.07	–[b]	–[b]
$[Ga^{III}Zn^{II}(H_2L^3)(solv)_x]^{4+}$	6.5 ± 0.1	10.9 ± 0.1	90.34 ± 13.87	13.03 ± 3.51	12 ± 4
$[Zn^{II}(H_3L^4)(solv)_x]$	(12.4)[c]	–	–	0.12 ± 0.04	1 ± 1
$[Zn^{II}_2(H_2L^4)(solv)_x]^{2+}$	–	–	–	n.a.	n.a.
$[Ga^{III}(H_2L^4)(solv)_x]^+$	6.7 ± 0.1	8.7 ± 0.2	0.01 ± 0.05	0.67 ± 0.14	7 ± 2
$[Ga^{III}Zn^{II}(H_2L^4)(solv)_x]^{3+}$	6.5 ± 0.2	10.5 ± 0.3	12.84 ± 3.62	1.83 ± 0.21	7 ± 1
$[Zn^{II}_2(H_2L^5)(OAc)_2]^+$ [16]	7.7	9.5	4.19 ± 0.67	0.09 ± 0.01	2 ± 1

[a] Assays in aqueous buffer solution pH = 7.
[b] Kinetic data for $[Ga^{III}(H_2L^3)(solv)_x]^+$ could not be determined as Michaelis–Menten behavior was not observed.
[c] pK_a values close to limits of the examined pH range.

initial hydrolysis rate. However, the initial hydrolysis rate of $[Zn^{II}(H_2L^3)(solv)_x]^+$ is higher at pH 10 than that of $[Zn^{II}(H_3L^4)(solv)_x]^+$, indicating an increase of the pK_a by the pivaloyl-amide residue adjacent to the Zn^{II} center. This is supported by the observation that $[Zn^{II}_2(H_2L^4)(solv)_x]^{2+}$ is active at higher pH than $[Zn^{II}_2(H_2L^3)(solv)_x]^{3+}$, and the increase of the initial hydrolysis rate with increasing pH from 9 to 10 for the latter is more pronounced. The differences in the catalytic behavior of $[Zn^{II}_2(H_2L^3)(solv)_x]^{3+}$ and $[Zn^{II}_2(H_2L^4)(solv)_x]^{2+}$ might be a synergistic outcome of (i) the different primary coordination sphere, and (ii) the different positioning of the hydrogen bond donors in the second coordination sphere.

Comparison of the Zn^{II}_2 complexes of H_3L^5 and H_4L^4 provides the opportunity to study the effect of changes to the first coordination sphere with similar secondary coordination spheres. While H_3L^5 has two N_3O binding sites, H_4L^4 offers an N_3O- and an N_2O_2-coordination site [16,24]. $[Zn^{II}_2(H_2L^5)(\mu\text{-}OAc)_2]^+$ and $[Zn^{II}_2(H_2L^4)(solv)_x]^{2+}$ exhibit similar behavior of their BDNPP hydrolysis activity; with increasing pH the initial hydrolysis rate for both increases significantly [16]. However, the initial hydrolysis rate measured at pH 9 is significantly higher for $[Zn^{II}_2(H_2L^4)(solv)_x]^{2+}$ than for $[Zn^{II}_2(H_2L^5)(\mu\text{-}OAc)_2]^+$, and this is attributed to the substitution of one pyridine donor by a more basic terminal phenolate. Therefore, the higher initial hydrolysis rate of $[Zn^{II}_2(H_2L^4)(solv)_x]^{2+}$ compared to $[Zn^{II}_2(H_2L^3)(solv)_x]^{3+}$ is attributed to the more basic phenolate donor in the former complex.

The most pronounced difference between the asymmetric and symmetric isomeric ligands H_3L^3 and H_4L^4 emerges from the Ga^{III} complexes. The pH profiles shown in Fig. 6a illustrate that, over the entire pH range studied, $[Ga^{III}(H_2L^4)(solv)_x]^+$ and $[Ga^{III}Zn^{II}(H_2L^4)(solv)]^{3+}$ have significantly higher initial hydrolysis rates than the corresponding H_3L^3 systems.

The $Ga^{III}Zn^{II}$ complexes $[Ga^{III}Zn^{II}(H_2L^4)(solv)]^{3+}$ and $[Ga^{III}Zn^{II}(H_2L^3)(solv)]^{4+}$ differ in two structural features, (i) the primary coordination environment at the Ga^{III} center, and (ii) the position of the hydrogen bond donors, mimicking the histidine residues in the second coordination sphere of the PAP active site (see Chart 4). The results of the phosphoester hydrolysis study of the previously reported complex $[Ga^{III}Zn^{II}(L^2)(\mu\text{-}OAc)_2]^+$ help to extract the impact of the structural variations [7]. The Ga^{III} environment in $[Ga^{III}Zn^{II}(H_2L^4)(solv)]^{3+}$ and $[Ga^{III}Zn^{II}(L^2)(\mu\text{-}OAc)_2]^+$ is similar with respect to the primary coordination sphere but differ in the secondary coordination sphere as only $[Ga^{III}Zn^{II}(H_2L^4)(solv)]^{3+}$ has a pivaloyl-amide residue adjacent to the Ga^{III} center. The Ga^{III} centers in both $[Ga^{III}Zn^{II}(H_2L^3)(solv)]^{4+}$ and $[Ga^{III}Zn^{II}(L^2)(\mu\text{-}OAc)_2]^+$ do not have a hydrogen bond donor in close proximity and, therefore, do not vary in the secondary coordination sphere. However, the primary coordination spheres of the two complexes are different. Therefore, the comparison of the kinetic parameters of $[Ga^{III}Zn^{II}(H_2L^4)(solv)]^{3+}$ and $[Ga^{III}Zn^{II}(L^2)(\mu\text{-}OAc)_2]^+$ facilitates the elucidation of the catalytic effect of a hydrogen bonding donor adjacent to the Ga^{III} center. Similarly, comparison of $[Ga^{III}Zn^{II}(H_2L^3)(solv)]^{4+}$ and $[Ga^{III}Zn^{II}(L^2)(\mu\text{-}OAc)_2]^+$ gives an insight in the impact of the exchange of a pyridine by a phenolate residue in the primary coordination environment of the Ga^{III} center.

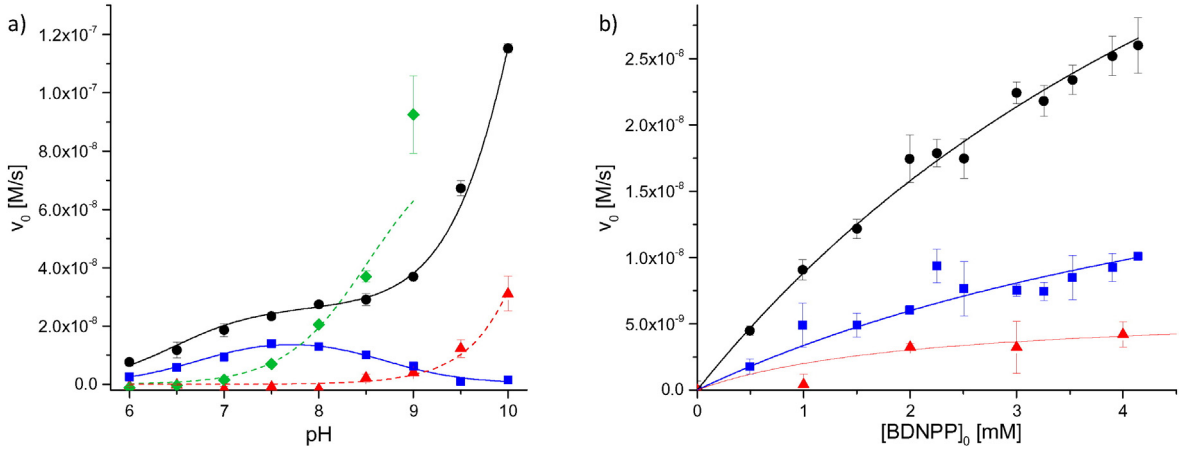

Fig. 5. a) pH dependence (0.04mM in complex, 5mM in BDNPP) and b) substrate concentration dependence at pH = 7 (0.04mM in complex) of BDNPP hydrolysis activity formixtures of ligand H_4L^4 with 1 eq Zn^{II} (red triangles), 2 eq Zn^{II} (green diamonds), 1 eq Ga^{III} (blue squares), or 1 eq Ga^{III} followed by 1 eq Zn^{II} (black circles).

Please cite this article as: S. Bosch, et al., Asymmetric mono- and dinuclear GaIII and ZnII complexes as models for purple acid phosphatases, J. Inorg. Biochem. (2016), http://dx.doi.org/10.1016/j.jinorgbio.2015.12.028

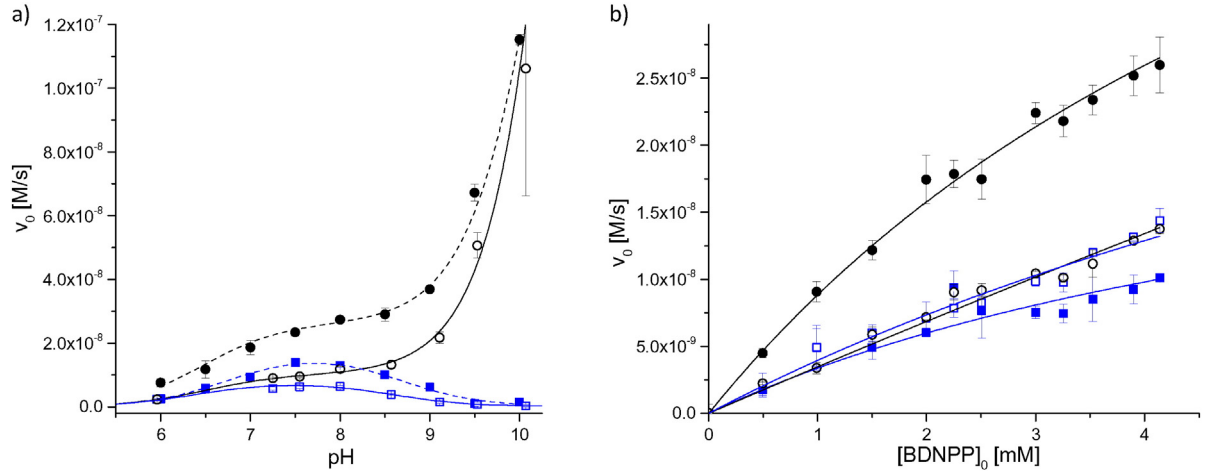

Fig. 6. Comparison of a) pH dependence (0.04mM in complex, 5mM in BDNPP) and b) substrate concentration dependence at pH = 7 (0.04mM in complex) of BDNPP hydrolysis activity for mixtures of ligand H_3L^3 (unfilled symbols) and H_4L^4 (filled symbols) with 1 eq Ga^{III} (blue squares), or 1 eq Zn^{II} followed by 1 eq Ga^{III} (black circles).

In contrast to $[Ga^{III}Zn^{II}(H_2L^3)(solv)_x]^{4+}$ and $[Ga^{III}Zn^{II}(H_2L^4)(solv)_x]^{3+}$, $[Ga^{III}Zn^{II}(L^2)(\mu\text{-}OAc)_2]^{+}$ exhibits a sigmoidal v_0 vs. pH curve with a relatively sharp activity maximum at pH ~ 6.8 [7]. The differences in the pH profiles observed for $[Ga^{III}Zn^{II}(H_2L^3)(solv)_x]^{4+}$ and $[Ga^{III}Zn^{II}(H_2L^4)(solv)_x]^{3+}$ on the one hand and $[Ga^{III}Zn^{II}(L^2)(\mu\text{-}OAc)_2]^{+}$ on the other are attributed to the hydrogen bond donors adjacent to the Zn^{II} site. The Ga^{III} sites in $[Ga^{III}Zn^{II}(H_2L^3)(solv)_x]^{4+}$ and $[Ga^{III}Zn^{II}(L^2)(\mu\text{-}OAc)_2]^{+}$ do not provide hydrogen bonding but they differ in the primary coordination sphere. The Ga^{III} center in $[Ga^{III}Zn^{II}(H_2L^3)(solv)_x]^{4+}$ is bound in a N_3O-site, while the Ga^{III} ion in $[Ga^{III}Zn^{II}(L^2)(\mu\text{-}OAc)_2]^{+}$ is coordinated to a N_2O_2-site. Therefore, the shift of the pH maximum by 0.8 pH units with respect to the phosphoester hydrolysis activity in the region between pH 7 and pH 9 to more acidic conditions is proposed to be a result of the electron-rich phenolate donor. However, we note that this is in contrast to results obtained with the monogallium(III) complexes of a series of tripodal ligands [25].

The Ga^{III} ions in $[Ga^{III}Zn^{II}(H_2L^4)(solv)_x]^{3+}$ and $[Ga^{III}Zn^{II}(L^2)(\mu\text{-}OAc)_2]^{+}$ have both the same primary coordination sphere but in $[Ga^{III}Zn^{II}(H_2L^4)(solv)_x]^{3+}$, in contrast to the L^2-based system, a pivaloyl-amide residue is positioned adjacent to the Ga^{III} site. The pH maximum for the hydrolysis activity in the region between pH 7 and pH 9 is shifted by 0.7 pH units to more basic conditions by the incorporation of a hydrogen bond donor proximal to the Ga^{III} center. Therefore, the capacity of hydrogen bonding has a similar effect as a less electron-rich ligand in the primary coordination sphere, resulting in a more basic activity maximum.

Although the pH maxima of the hydrolysis activity in the region between pH 6 and pH 9 are shifted to more basic conditions for the two complexes with hydrogen bond donors proximal to the dinuclear core, at pH 7 $[Ga^{III}Zn^{II}(H_2L^3)(solv)]^{4+}$ and $[Ga^{III}Zn^{II}(H_2L^4)(solv)]^{3+}$ (see Table 3) exhibit (i) higher hydrolysis rates k_{cat}, and (ii) higher K_M values, i.e. lower substrate affinity than $[Ga^{III}Zn^{II}(L^2)(\mu\text{-}OAc)_2]^{+}$ (see Table 2), which lacks hydrogen bonding capacity [7]. Moreover, the positioning of two hydrogen bond donors adjacent to the Zn^{II} binding site has the most pronounced effect.

2.3.4. Turn over numbers (TONs)

TONs of the Zn^{II}, Zn^{II}_2, Ga^{III}, and $Ga^{III}Zn^{II}$ complexes of H_3L^3 and H_4L^4 were determined in assays as described for the kinetic studies in aqueous-buffer solution at pH 7, followed over 9 days (see Section 4). The data are listed in Table 4 and a graphical presentation appears as Supporting Information. With the monozinc(II) complexes $[Zn^{II}(H_2L^3)(solv)_x]^{+}$ and $[Zn^{II}(H_3L^4)(solv)_x]^{+}$, the acceleration of hydrolysis appears to be similar in the first 60 h. However, $[Zn^{II}(H_3L^4)(solv)_x]^{+}$ with a Zn^{II} adjacent to a hydrogen bond donor is inhibited at lower product concentration than $[Zn^{II}(H_2L^3)(solv)_x]^{+}$ that has no hydrogen bond donors proximal to the Zn^{II} center.

A similar result emerges from the Ga^{III} data, i.e. $[Ga^{III}(H_2L^4)(solv)_x]^{+}$ with a pivaloyl-amide residue adjacent to the Ga^{III} center has higher TONs than $[Ga^{III}(H_2L^3)(solv)_x]^{2+}$. However, compared to the monozinc(II) complexes both monogallium(III) systems exhibited higher TONs, as expected from the kinetic studies. Therefore, inhibition by the phosphomonoester product in the mononuclear complexes is more pronounced with Zn^{II} than Ga^{III} and is enhanced by proximal hydrogen bond donors. The $Ga^{III}Zn^{II}$ complex $[Ga^{III}Zn^{II}(H_2L^3)(solv)_x]^{4+}$ with two privaloyl-amide residues proximal to the Zn^{II} center exhibits a lower TON than the isomer with a symmetric disposition of the pivaloyl groups. This suggests that steric hindrance does not prevent inhibition. The higher TON of $[Ga^{III}Zn^{II}(H_2L^4)(solv)_x]^{3+}$ is assumed to be due to the lower product affinity of the Ga^{III} center coordinated to the electron-rich terminal phenolate residue.

The heterodinuclear complex $[Ga^{III}Zn^{II}(H_2L^4)(solv)_x]^{3+}$ reveals a higher TON than the homodinuclear complex $[Zn^{II}_2(H_2L^4)(solv)_x]^{2+}$. It appears that a phosphoester bridge between two Zn^{II} centers coordinated in H_4L^4 is more easily formed than between a Ga^{III} and a Zn^{II} center, i.e. at lower product concentration. Interestingly, the TON of $[Ga^{III}Zn^{II}(H_2L^4)(solv)_x]^{3+}$ is also higher than for the two mononuclear complexes $[Zn^{II}(H_3L^4)(solv)_x]^{+}$ and $[Ga^{III}(H_2L^4)(solv)_x]^{+}$, indicating a positive interaction of the two metal ions in the heterodinuclear complex.

Comparing the different complexes of H_3L^3 without a terminal phenolate, the results suggest that the heterodinuclear complex $[Ga^{III}Zn^{II}(H_2L^3)(solv)_x]^{4+}$ exhibits a similar TON as the dizinc(II) complex $[Zn^{II}_2(H_2L^3)(solv)_x]^{3+}$, indicating that the inhibition is

Table 4
TONs of BDNPP hydrolysis with H_3L^3 or H_4L^4 with 1 eq Zn^{II}, 2 eq of Zn^{II}, 1 eq Ga^{III}, 1 eq Ga^{III} followed by 1 eq Zn^{II} (all kinetic studies in a mixture of acetonitrile:aqueous buffer solution (1:1)).

Complex	TON[a]
$[Zn^{II}(H_2L^3)(solv)_x]^{+}$	10 ± 1
$[Zn^{II}_2(H_2L^3)(solv)_x]^{3+}$	18 ± 1
$[Ga^{III}(H_2L^3)(solv)_x]^{2+}$	35 ± 1
$[Ga^{III}Zn^{II}(H_2L^3)(solv)_x]^{4+}$	23 ± 5
$[Zn^{II}(H_3L^4)(solv)_x]$	6 ± 1
$[Zn^{II}_2(H_2L^4)(solv)_x]^{2+}$	16 ± 1
$[Ga^{III}(H_2L^4)(solv)_x]^{+}$	21 ± 1
$[Ga^{III}Zn^{II}(H_2L^4)(solv)_x]^{3+}$	25 ± 2

[a] Assays with aqueous buffer solution pH = 7, TONs determined after 9 days.

Please cite this article as: S. Bosch, et al., Asymmetric mono- and dinuclear GaIII and ZnII complexes as models for purple acid phosphatases, J. Inorg. Biochem. (2016), http://dx.doi.org/10.1016/j.jinorgbio.2015.12.028

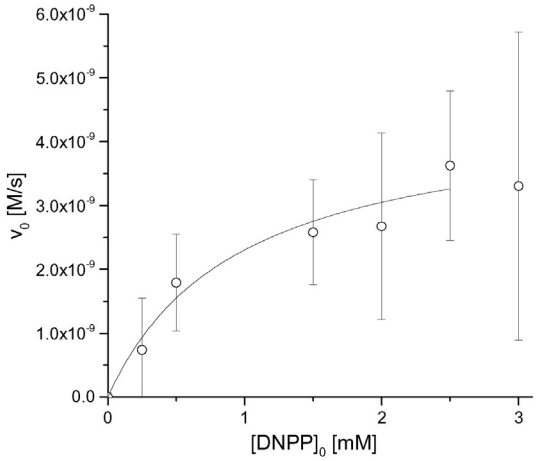

Fig. 7. Substrate concentration dependence at pH = 7 of DNPP hydrolysis for H_3L^3 with 1 eq Zn^{II} and 1 eq of Ga^{III} (complex concentration of 0.04 mM; only the first 5 points were considered for the fit).

independent of the two metal ions bound in the two binding sites of H_3L^3. However, $[Ga^{III}Zn^{II}(H_2L^3)(solv)_x]^{4+}$ shows a sharper increase of the absorbance at 400 nm with time, especially in the first 40 h, compared to $[Zn^{II}_2(H_2L^3)(solv)_x]^{3+}$. Therefore, the hydrolysis rate depends significantly on the presence of the trivalent metal ion.

It emerges that the $Ga^{III}Zn^{II}$ complex of H_4L^4 is the most active catalyst; in contrast to H_3L^3, where the monogallium(III) complex is most active. Surprisingly, $[Ga^{III}(H_2L^3)(solv)_x]^{2+}$ exhibits the highest TON of all complexes studied, with a TON of 35 after nine days. The relatively high TON of $[Ga^{III}(H_2L^3)(solv)_x]^{2+}$ is ascribed to the lower product affinity of Ga^{III} compared to Zn^{II}, the lack of a proximal hydrogen bond donor, and the absence of a second metal ion and the resulting inability to efficiently bind the phosphomonoester product (inhibition).

2.3.5. Phosphomonoester hydrolysis

The phosphomonoester hydrolysis activity of the Zn^{II}, Zn^{II}_2, Ga^{III} and $Ga^{III}Zn^{II}$ complexes of H_3L^3 and H_4L^4 was studied with the activated model substrate DNPP (2,4-dinitrophenylphosphate) at different pHs (7, 8, 9 and 10). A significant phosphomonoester hydrolysis capacity was only observed for $[Ga^{III}Zn^{II}(H_2L^3)(solv)_x]^{4+}$, and only a slight increase in the 2,4-phenolate concentration was observed in the assays with $[Ga^{III}(H_2L^3)(solv)_x]^{4+}$ at pH 7 and $[Zn^{II}_2(H_2L^4)(solv)_x]^{2+}$ at pH 9.5, compared to autohydrolysis. However, due to the instability of DNPP in the buffer solutions, the deviations of the initial hydrolysis rates, obtained from the measurements with $[Ga^{III}(H_2L^3)(solv)_x]^{4+}$ and $[Zn^{II}_2(H_2L^4)(solv)_x]^{2+}$, are too high for a quantitative analysis.

The fact that only the $Ga^{III}Zn^{II}$ and Ga^{III} complexes of H_3L^3 are able to hydrolyze the phosphomonoester DNPP, therefore contrasting the corresponding H_4L^4 systems, indicates that neither the strong electron-rich terminal phenolate nor the hydrogen bond donor proximal to the trivalent metal center lead to the capacity of phosphomonoester hydrolysis in PAPs. Moreover, the dizinc(II) complex of H_3L^3 did not reveal phosphomonoester hydrolysis. This indicates that the trivalent metal ion is essential for the DNPP hydrolysis. The only model complexes reported so far to cleave phosphomonoester bonds contained at least one Fe^{III} ion [24,26].

The substrate concentration dependence was measured at pH 7 in order to mimic near physiological conditions (Fig. 7). $[Ga^{III}Zn^{II}(H_2L^3)(solv)_x]^{4+}$ shows Michaelis–Menten type behavior and yields $k_{cat} = (0.11 \pm 0.02)\cdot 10^{-3}\ s^{-1}$ and $K_M = (0.96 \pm 0.37)$ mM. Although the activity of $[Ga^{III}Zn^{II}(H_2L^3)(solv)_x]^{4+}$ is lower than those reported for the corresponding diiron complexes [24,26], $[Ga^{III}Zn^{II}(H_2L^3)(solv)_x]^{4+}$ is to date the first heterodinuclear model complex able to hydrolyze phosphomonoesters.

3. Conclusion

The complexes described here combine the three essential structural features of the active site of PAPs: (i) a distinct coordination environment in two adjacent binding sites, (ii) a mixed-valent dinuclear metal core, and (iii) a hydrogen bonding network provided by the second coordination sphere (Chart 2). With hydrogen bond donors proximal to the metal centers that model the non-coordinating histidine residues in the active site of PAPs, the impact of the hydrogen bonding capacity on the reactivity has been examined by comparing the catalytic properties of the series complexes, also including the previously reported $[Ga^{III}Zn^{II}(L^2)(\mu\text{-}OAc)_2]^+$ catalyst [7].

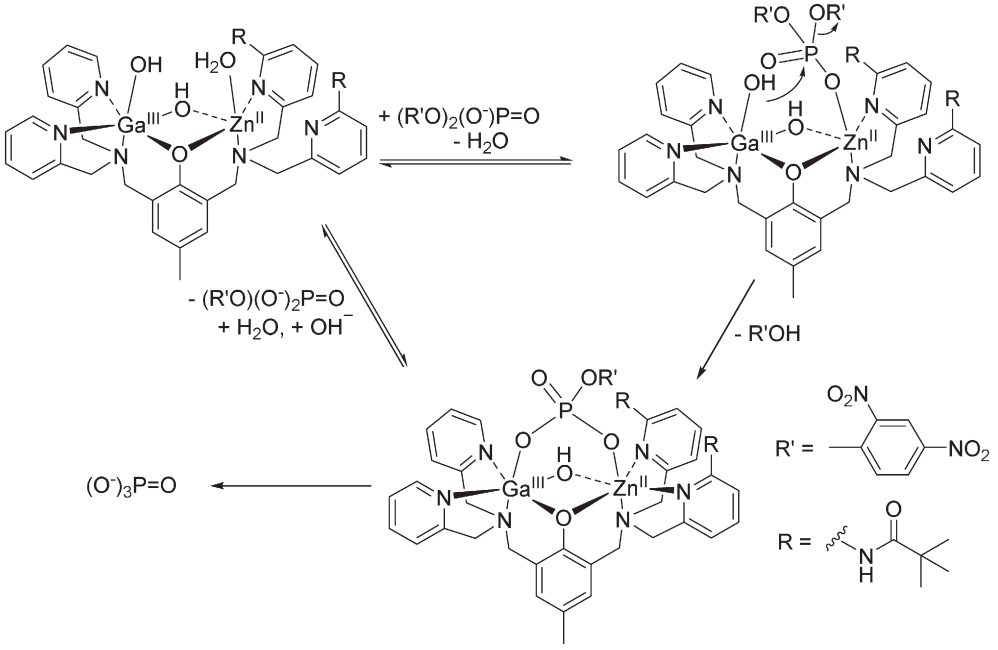

Scheme 3. Proposed mechanism for the BDNPP hydrolysis catalyzed by $[Ga^{III}Zn^{II}(H_2L^3)(solv)_x]^{4+}$.

The mechanism that emerges involves an initial monodentate coordination of the substrate to the divalent metal ion, followed by a nucleophilic attack by the terminal M^{III}-bound hydroxide. This is supported by reported kinetic isotope effects and UV–vis spectroscopic substrate binding studies in similar systems, i.e. $[Fe^{III}Co^{II}(L^2)(\mu\text{-}OAc)_2]^+$ and $[Ga^{III}Co^{II}(L^2)(\mu\text{-}OAc)_2]^+$ [9].

The influence of the nature of the donor sites on the reactivity of Ga^{III} as a model of the Fe^{III} ion in PAPs has been evaluated with monogallium(III) complexes of tripodal ligands [25]. Attack of the coordinated substrate by a Ga^{III}-bound hydroxide was shown to be directly involved in the catalytic mechanism as a nucleophile rather than acting as a general base for an incoming water which, upon deprotonation, attacks the phosphoester substrate [25].

The results of the mono- and dinuclear complexes of the two asymmetric ligands H_3L^3 and H_4L^4 with differing primary and secondary coordination spheres lead to a deeper insight in the reaction mechanism of phosphoester hydrolysis with heterodinuclear biomimetics. In the proposed mechanism, the phosphoester is fixed and activated by the Zn^{II} center, and the Ga^{III} site is responsible for providing the hydroxide nucleophile at near physiological conditions (Scheme 3).

It emerges that the monozinc(II) complexes are not able to hydrolyze phosphoesters at near physiological conditions but coordination of a second Zn^{II} ion in the same catalyst enables the reaction. A similar cooperative effect of the metal ions is observed in the $Ga^{III}Zn^{II}$ complexes. Although the substrate affinity of the complex $[Ga^{III}Zn^{II}(H_2L^3)(solv)_x]^{4+}$ is lower than that of the corresponding Zn^{II}_2 complex, the heterodinuclear complex exhibits a 23-fold faster hydrolysis and an approx. sevenfold increased efficiency. Comparison of the activity of the two different $Ga^{III}Zn^{II}$ complexes reveals a shift of the optimum pH to higher values with an electron-poor donor in the primary coordination sphere or provision of hydrogen bonding by the second coordination sphere. The capacity of a hydrogen bonding network proximal to the dinuclear core results in higher hydrolysis rates, lower substrate affinities, and higher efficiencies, especially when the two hydrogen bond donors are proximal to the Zn^{II} center. However, studies over a longer time period indicate that a crowded active site does not efficiently prevent inhibition. The experiments at a longer time scale also indicate an acceleration by the trivalent metal ion. Also, a phenolate coordinated to Ga^{III} in comparison with pyridine results in an increase of the turnover. However, the highest TON was found for the monogallium(III) complex without hydrogen bond donors in close distance to the metal center but with a vacant second amidated coordination site.

The results of the DNPP hydrolysis of the different complexes show that only $[Ga^{III}Zn^{II}(H_2L^3)(solv)_x]^{4+}$ is able to cleave phosphomonoesters efficiently. Therefore, this complex does not only combine the essential structural features of the active site of PAP, but is also the first heterodinuclear model complex mimicking the essential function of PAPs, i.e. the hydrolysis of phosphomonoesters.

4. Experimental section

4.1. Syntheses

4.1.1. Ligand syntheses

Ligand H_3L^3 [16], *N*-(6-(((pyridin-2-ylmethyl)amino)methyl)pyridin-2-yl)pivalamide (1) [24,27,28], 3-(chloromethyl)-2-hydroxy-5-methylbenzaldehyde (2) [29,30], 2-(aminomethyl)phenol (4) [31], *N*-(6-(bromomethyl)pyridin-2-yl)pivalamide (6) [27,32–34], BDNPP [35], and DNPP [36] were prepared as described previously

4.1.1.1. Compound 3. *N*-(6-pivaloylamido-2-pyridylmethyl)-*N*-(2-pyridylmethyl)amine (1) (4.92 g, 16.5 mmol, 1.0 eq) was dissolved in anhydrous dichloromethane (26.5 ml) and treated with triethylamine (4.30 ml, 3.09 g, 16.5 mmol, 1.0 eq). This solution was then added dropwise to a cold mixture of 3-(chloromethyl)-2-hydroxy-5-methylbenzaldehyde (2) (3.05 g, 16.5 mmol, 1.0 eq) in tetrahydrofuran (30.0 ml) at 0 °C. Afterwards the mixture was stirred for two days at room temperature and the white precipitate obtained was filtered, washed with a small amount of dichloromethane and the filtrate was concentrated under reduced pressure. The remaining yellow oil was taken up in dichloromethane (50 ml), washed with half concentrated brine (20 ml) and dried over sodium sulfate. The solvent was evaporated under vacuum to yield compound 3 as a yellow solid (7.07 g, 96%). HRMS (ESI^+, CH_3OH): m/z = 447.2391 ($[C_{26}H_{31}N_4O_3]^+$, *calcd.* 447.2391). ^1H NMR (399.89 MHz, $CDCl_3$): δ = 1.38 (s, 9 H, *H*24), 2.29 (s, 3 H, *H*17), 3.81 (s, 2 H, *H*13), 3.89 (s, 4 H, *H*6, *H*12), 6.98 (d, ^3J = 7.53 Hz, 1 H, *H*10), 7.15 (dd, ^3J = 7.28 Hz, ^3J = 5.24 Hz, 1 H, *H*2), 7.20 (d, ^4J = 1.51 Hz, 1 H, *H*15), 7.37 (d, ^3J = 7.91 Hz, 1 H, *H*4), 7.49 (d, ^4J = 1.63 Hz, 1 H, *H*18), 7.60–7.67 (m, 2 H, *H*3, *H*9), 8.14 (d, ^3J = 8.28 Hz, 1 H, *H*8), 8.46 (bs, 1 H, N*H*), 8.52 (d, ^3J = 4.77 Hz, 1 H, *H*1), 10.52 (s, 1 H, *H*21), 11.74 (bs, 1 H, O*H*) ppm. ^{13}C NMR (100.55 MHz, $CDCl_3$): δ = 20.2 (*C*17), 27.4 (*C*24), 39.8 (*C*23), 55.7 (*C*13), 58.3 (*C*12), 59.4 (*C*6), 112.0 (*C*8), 118.0 (*C*10), 122.2 (*C*2), 122.9 (*C*4), 125.0 (*C*14), 128.1 (*C*16, *C*19), 128.3 (*C*18), 136.8 (*C*3), 137.8 (*C*15), 139.2 (*C*9), 148.8 (*C*1), 151.3 (*C*7), 156.1 (*C*11), 158.2 (*C*5), 158.7 (*C*20), 177.2 (*C*22), 191.1 (*C*21) ppm.

4.1.1.2. Compound 5. A mixture of compound 3 (6.25 g, 14.0 mmol, 1.0 eq) and 2-(aminomethyl)phenol (4) (2.42 g, 19.6 mmol, 1.4 eq) in methanol (300 ml) was heated at 50 °C for three hours. The solution was cooled with an ice-water bath and sodium borohydride (1.99 g, 52.6 mmol, 3.8 eq) was added in portions. After addition, the reaction mixture was refluxed for three hours. After cooling to room temperature the solution was concentrated under vacuum. The remaining oil was taken up in dichloromethane (100 ml) and saturated sodium bicarbonate solution (100 ml) was added carefully. Using solid sodium carbonate the pH value was adjusted to 14. The phases were separated and the aqueous phase was extracted with dichloromethane (4 × 75 ml). The combined organic phases were washed with brine (20 ml) and dried over sodium sulfate. Removal of the solvent yielded compound 5 as a yellowish solid which was used in the next step without further purification. HRMS (ESI^+, CH_3OH): *m/z* = 554.3125 ($[C_{33}H_{40}N_5O_3]^+$, *calcd.* 554.3126). ^1H NMR (200.13 MHz, $CDCl_3$): δ = 1.27 (s, 6 H, $(CH_3)C$), 1.30 (s, 3 H, $(CH_3)C$), 2.17 (s, 3 H, CH_3), 3.66 (s, 2 H, CH_2), 3.75 (s, 2 H, CH_2), 3.77 (s, 2 H, CH_2), 3.82 (s, 2 H, CH_2), 3.86 (s, 2 H, CH_2), 4.69 (s, 1 H, $N_{amin}H$), 6.76 (td, ^3J = 7.32, ^4J = 1.21, 1 H, H_{aryl}), 6.84–6.94 (m, 4 H, H_{aryl}), 7.03 (s, 1 H, H_{aryl}), 7.09–7.22 (m, 3 H, H_{aryl}), 7.26–7.34 (m, 1 H, H_{aryl}), 7.52–7.68 (m, 2 H, H_{aryl}), 8.13 (d, ^3J = 8.34, 2 H, H_{aryl}), 8.45 (s, 1 H, $N_{amid}H$), 8.51 (ddd, ^3J = 4.89, ^4J = 1.86, ^5J = 0.82, 1 H, H_{aryl}) ppm.

4.1.1.3. Ligand H_4L^4. Compound 5 (7.75 g, 14.0 mmol, 1.0 eq) was dissolved in acetonitrile (400 ml) and treated with sodium carbonate (1.48 g, 14.0 mmol, 1.0 eq). Then, *N*-(6-bromomethyl)pyridine-2-yl)pivalamide (6) (3.80 g, 14.0 mmol, 1.0 eq) was added and the reaction mixture was stirred at room temperature for 24 h. The solution was concentrated to a brown oil, which was taken up in dichloromethane (100 ml) and saturated sodium bicarbonate solution (100 ml). The product was extracted into dichloromethane (4 × 50 ml), washed with brine (30 ml) and dried over sodium sulfate. After removal of the solvent the crude product was purified via column chromatography (SiO_2; DEE:*n*-hexane:NH_3 (7 N in MeOH) = 90:8:2; R_f = 0.48) to yield H_4L^4 as yellowish solid (2.12 g, 22%). HRMS (ESI^+, CH_3OH): *m/z* = 744.4237 ($[C_{44}H_{54}N_7O_4]^+$, *calcd*. 744.4232). ^1H NMR (500.13 MHz, CD_3CN): δ = 1.28 (s, 9 H, *H*36/*H*39), 1.28 (s, 9 H, *H*36/*H*39), 2.13 (s, 3 H, *H*17), 3.67 (s, 2 H, *H*13/21), 3.73 (s, 2 H, *H*13/21), 3.74 (s, 4 H, *H*6, *H*27/*H*30), 3.76 (s, 2 H, *H*27/*H*30), 3.77 (s, 2 H, *H*12), 6.74–6.79 (m, 2 H, *H*7/*H*9), 6.81 (d, ^4J = 1.83 Hz, 1 H, *H*15/*H*18), 6.84 (dd, ^3J = 7.70 Hz, ^4J = 0.73 Hz, 1 H, *H*25/*H*31), 6.96 (d, ^4J = 2.20 Hz, 1 H, *H*15/*H*18), 6.99 (dd, ^3J = 7.70 Hz, ^4J = 0.73 Hz, 1 H, *H*25/*H*31), 7.09 (dd, ^3J = 7.34 Hz, ^4J = 1.47 Hz, 1 H, *H*10), 7.12–7.15 (m, 2 H,

*H*2/*H*8), 7.33 (d, $^3J = 7.70$ Hz, 1 H, *H*4), 7.56–7.61 (m, 2 H, H3, *H*24/*H*30), 7.64 (t, $^3J = 7.89$ Hz, 1 H, *H*24/*H*30), 7.97 (d, $^3J = 8.07$ Hz, 1 H, *H*23/*H*29), 8.00 (d, $^3J = 7.70$ Hz, 1 H, *H*23/*H*29), 8.42 (bs, 1 H, N*H*), 8.45 (ddd, $^3J = 4.86$ Hz, $^4J = 1.82$ Hz, $^5J = 0.84$ Hz, 1 H, *H*1), 8.48 (bs, 1 H, N*H*) ppm. ^{13}C NMR (125.76 MHz, CD_3CN): $\delta = 20.6$ (*C*17), 27.6 (*C*36/*C*39), 27.7 (*C*36/*C*39), 40.5 (*C*35/*C*38), 40.5 (*C*35/*C*38), 52.9 (*C*13/*C*21), 57.2 (*C*13/*C*21), 58.0 (*C*12), 58.7 (*C*27/*C*33), 59.0 (*C*27/*C*33), 59.8 (*C*6), 112.3 (*C*23/*C*29), 112.4 (*C*23/*C*29), 116.8 (*C*7/*C*9), 119.1 (*C*25/*C*31), 119.3 (*C*25/*C*31), 119.9 (*C*7/*C*9), 123.1 (*C*2), 123.9 (*C*4), 124.29 (*C*14/*C*20), 124.4 (*C*11), 124.9 (*C*14/*C*20), 128.5 (*C*16), 129.7 (*C*8), 131.0 (*C*10, *C*15/*C*18), 131.1 (*C*10, *C*15/*C*18), 131.4 (*C*10, *C*15/*C*18), 137.6 (*C*3), 140.0 (*C*24/*C*30), 140.0 (*C*24/*C*30), 149.8 (*C*1), 152.3 (*C*22/*C*28), 152.4 (*C*22/*C*28), 154.5 (*C*20), 157.7 (*C*26/*C*32), 157.9 (*C*26/*C*32), 158.6 (*C*7a), 159.6 (*C*5), 177.9 (*C*34/*C*37). FT-IR spectroscopy: $\nu = 3669$ (ν{OH}), 3388 (ν{N-H}), 2971 (ν{C-H}), 2901 (ν{C-H}), 2819 (ν{C-H}), 1688 (ν{C = O}), 1520 (ν{C-N}, δ{CNH}), 1449 (ν{C-$(CH_3)_3$}), 755 (δ{py-H}) cm^{-1}. Elemental analysis: *Calcd*. for $C_{44}H_{53}N_7O_4$: C 71.04%, H 7.18%, N 13.18%; Found: C 70.66%, H 7.31%, N 13.35%.

4.2. Methods

4.2.1. NMR spectroscopy

^{1}H NMR spectra were recorded with a Bruker AV500 instrument. ^{13}C NMR and temperature-dependent spectra were measured with a Bruker AV400 instrument. Chemical shifts of ^{1}H and ^{13}C NMR spectra are reported in ppm, relative to known solvent peak references. For ^{31}P NMR spectra 85% phosphoric acid was used as the external reference. Two-dimensional correlation spectroscopy (COSY), nuclear Overhauser-effect spectroscopy (NOESY), heterodinuclear single quantum correlation (HSQC) and hetereodinuclear multiple bond connectivity (HMBC) experiments were used to assign each signal in the spectra. The following abbreviations were used: s (singlet), bs (broad singlet), d (doublet), dd (doublet of doublet), ddd (doublet of doublet of doublet), t (triplet), dt (doublet of triplet), sep (septet) and m (multiplet). Coupling constants are given in Hz. The spectra were obtained from CD_3CN solutions, and the chemical shifts were determined relative to the solvent peak. NOESY, COSY, HSQC and HMBC experiments were used to assign each signal in the spectra.

4.2.2. Mass spectrometry

High resolution mass spectra were collected with a Bruker microTOFQ ESI-MS spectrometer by Mr. Graham Macfarlane at the University of Queensland or with a Finnigan LCQ spectrometer at the Institute of Organic Chemistry at the University of Heidelberg and processed with Bruker Compass Data Analysis software.

4.2.3. FT-Infrared spectroscopy

Spectra were measured with a Perkin Elmer FT-IR Spectrometer SPECTRUM 2000 with a Smiths DuraSamplIR II ATR diamond window.

4.2.4. UV–vis-NIR spectroscopy

The spectra were recorded at 25 °C with a TIDAS II J&M spectrophotometer and a JASCO V-570 spectrophotometer in 10 mm quartz cuvettes

4.2.5. Elemental microanalyses

Were performed in the analytic laboratories of the Institute of Chemistry at the University of Heidelberg with an Elementar Vario EL machine.

4.2.6. Kinetic experiments

Cleavage of the phosphorous–oxygen bond was followed at 25 °C by monitoring the product generated, 2,4-dinitrophenolate, by its strong absorption at 400 nm ($\varepsilon = 12{,}100\ M^{-1}\ cm^{-1}$). All measurements were carried out in 1:1 acetonitrile–buffer mixtures and performed in triplicate. The aqueous buffer consisted of 2-(*N*-morpholino)ethanesulfonic acid (MES) (50 mM; pH range: 5.5–6.7), 4-(2-hydroxyethyl)piperazine-1-ethanesulfonic acid (HEPES) (50 mM; pH range: 6.8–8.2), 2-(cyclohexylamino)ethanesulfonic acid (CHES) (50 mM; pH range: 8.6–10.0), 3-(cyclohexylamino)-1-propanesulfonic acid (CAPS) (50 mM; pH range: 9.7–11.1) and lithium perchlorate (250 mM) for ionic strength control. The desired pH of the buffers was adjusted by addition of aqueous sodium hydroxide solution. Following treatment with chelex® (Chelex 100 sodium form) overnight and filtration with 45 μm syringe filters ensured the absence of metal ions in the buffer solutions. The activated model substrate BDNPP was initially prepared as 15 mM stock solution in acetonitrile and the complex stock solutions were 1 mM in acetonitrile. The complex was allowed to equilibrate in the acetonitrile–buffer mixture for one minute prior addition of substrate. When the substrate was added to the reaction mixture the starting hydrolysis activity was monitored in the time between 15 and 195 s and analyzed by linear regression. For each experiment autohydrolysis assays were conducted by measuring the hydrolysis rate under the same conditions, but without complex, and were subtracted from the derived data. The pH dependence assays contained the complex at 0.04 mM and BDNPP at 5 mM in the cuvette. The substrate concentration dependence of the catalytic rate was examined with a fixed complex concentration of 0.04 mM, and the BDNPP concentration was varied. The phosphomonoester hydrolysis activity of DNPP was examined similar to the BDNPP assays but DNPP was initially dissolved in an aqueous buffer solution at the required pH value. The substrate concentration dependence measurements were 0.04 mM in complex, and the DNPP concentration was varied. The experimental data obtained were fitted in the Origin (OriginLab) program to the Michaelis–Menten equation. Studies of the turn over number (TON) were conducted 10 μM in complex and 3 mM in BDNPP. Samples were taken at various intervals during the experiment, diluted with solvent (final concentrations: 0.5 nM in complex and 0.15 mM in BDNPP), and their UV–vis spectra were recorded to determine the progress of phosphoester hydrolysis. The increase in the absorbance at 400 nm, assigned to the hydrolysis product 2,4-dinitrophenolate, was monitored over time and TON values were calculated using the Beer–Lambert Law.

Acknowledgments

Financial support by the German Science Foundation (DFG), the German Academic Exchange Program (DAAD) and the University of Heidelberg are gratefully acknowledged. GS acknowledges the Australian Research Council for the award of a Future Fellowship (FT120100694).

Appendix A. Supplementary data

The Supporting Information includes details of the spectroscopic characterization of the compounds used as well as details on the kinetic studies. Supplementary data associated with this article can be found in the online version, at doi:http://dx.doi.org/10.1016/j.jinorgbio.2015.12.028.

References

[1] N. Mitić, S.J. Smith, A. Neves, L.W. Guddat, L.R. Gahan, G. Schenk, Chem. Rev. 106 (2006) 3338–3363.
[2] J.L. Beck, L.A. McConachie, A.C. Summors, W.N. Arnold, J. De Jersey, B. Zerner, Biochim. Biophys. Acta Protein Struct. Mol. Enzymol. 869 (1986) 61–68.
[3] A. Durmus, C. Eicken, B.H. Sift, A. Kratel, R. Kappl, J. Huttermann, B. Krebs, Eur. J. Biochem. 260 (1999) 709–716.
[4] G. Schenk, Y. Ge, L.E. Carrington, C.J. Wynne, I.R. Searle, B.J. Carroll, S. Hamilton, J. De Jersey, Arch. Biochem. Biophys. 370 (1999) 183–189.
[5] G. Schenk, C.L. Boutchard, L.E. Carrington, C.J. Noble, B. Moubaraki, K.S. Murray, J. De Jersey, G. Hanson, S. Hamilton, J. Biol. Chem. 276 (2001) 19084–19088.
[6] G. Schenk, N. Mitić, G. Hanson, P. Comba, Coord. Chem. Rev. 257 (2013) 473–482 (Special Issue Ed Solomon).
[7] S.J. Smith, A. Casellato, K.S. Hadler, N. Mitić, M.J. Riley, A.J. Bortoluzzi, B. Szpoganicz, G. Schenk, A. Neves, L.R. Gahan, J. Biol. Inorg. Chem. 12 (2007) 1207–1220.
[8] M. Merkx, B.A. Averill, Biochemistry 37 (1998) 8490–8497.

[9] F.R. Xavier, A. Neves, A. Casellato, R.A. Peralta, A.J. Bortoluzzi, B. Szpoganicz, P.C. Severino, H. Terenzi, Z. Tomkowicz, S. Ostrovsky, W. Haase, A. Ozarowski, J. Krzystek, J. Telser, G. Schenk, L.R. Gahan, Inorg. Chem. 48 (2009) 7905–7921.
[10] G. Schenk, L.W. Guddat, Y. Ge, L.E. Carrington, D.A. Hume, S. Hamilton, J. De Jersey, Gene 250 (2000) 117–125.
[11] A. Neves, M. Lanznaster, A.J. Bortoluzzi, R.A. Peralta, A. Casellato, E.E. Castellano, P. Herrald, M.J. Riley, G. Schenk, J. Am. Chem. Soc. 129 (2007) 7486–7487.
[12] C. Piovezan, R. Jovito, A.J. Bortoluzzi, H. Terenzi, F.L. Fischer, P.C. Serverino, C.T. Pich, G.G. Azzolini, R.A. Peralta, L.M. Rossi, A. Neves, Inorg. Chem. 49 (2010) 2580–2582.
[13] M. Lanznaster, A. Neves, A.J. Bortoluzzi, B. Szpoganicz, E. Schwingel, Inorg. Chem. 41 (2002) 5641–5643.
[14] L.J. Daumann, L. Marty, G. Schenk, L.R. Gahan, Dalton Trans. 42 (2013) 9574–9584.
[15] L.J. Daumann, L.R. Gahan, P. Comba, G. Schenk, Inorg. Chem. 51 (2012) 7669–7681.
[16] S. Bosch, P. Comba, L.R. Gahan, G. Schenk, Inorg. Chem. 53 (2014) 9036–9051.
[17] P.V. Bernhardt, S. Bosch, P. Comba, L.R. Gahan, G.R. Hanson, V. Mereacre, C. Nobel, A.K. Powell, G. Schenk, H. Wadepohl, Inorg. Chem. 54 (2015) 7249–7263.
[18] S. Bosch, P. Comba, L.R. Gahan, G.R. Hanson, G. Schenk, H. Wadepohl, Chem. Eur. J. 21 (2015) 18269–18279.
[19] R. Peralta, A.J. Bortoluzzi, B. de Souza, R. Jovito, F.R. Xavier, R.A.A. Couto, A. Casellato, F. Nome, A. Dick, L.R. Gahan, G. Schenk, G.R. Hanson, F.C.S. de Paula, E.C. Pereira-Maia, S. Machado, P.C. Severino, C. Pich, F.L. Fischer, H. Terenzi, E.E. Castellano, A. Neves, M.J. Riley, Inorg. Chem. 49 (2010) 11421–11438.
[20] I.H. Segel, Enzyme Kinetics — Behavior and Analysis of Rapid Equilibrium and Steady-State Enzyme SystemsWiley-VCH New York 1975.
[21] A. Kantacha, R. Buchholz, S. Smith, G. Schenk, L. Gahan, J. Biol. Inorg. Chem. 16 (2011) 25–32.
[22] G. Feng, J.C. Mareque-Rivas, N.H. Williams, Chem. Commun. (2006) 1845–1847.
[23] J. Hernandez-Gil, S. Ferrer, E. Salvador, J. Calvo, E. Garcia-Espana, J.C. Mareque-Rivas, Chem. Commun. 49 (2013) 3655–3657.
[24] P. Comba, L.R. Gahan, V. Mereacre, G.R. Hanson, A.K. Powell, G. Schenk, M. Zajaczkowski-Fischer, Inorg. Chem. 51 (2012) 12195–12209.
[25] F. Coleman, M.J. Hynes, A. Erxleben, Inorg. Chem. 49 (2010) 6725–6733.
[26] P. Comba, L.R. Gahan, G.R. Hanson, V. Mereacre, C.J. Noble, A.K. Powell, I. Prisecaru, G. Schenk, M. Zajaczkowski-Fischer, Chem. Eur. J. 18 (2012) 1700–1710.
[27] B. Osmialowski, E. Kolehmainen, R. Dobosz, R. Gawinecki, R. Kauppinen, A. Valkonen, J. Koivukorpi, K. Rissanen, J. Phys. Chem. 114 (2010) 10421–10426.
[28] T. Inomata, K. Shinozaki, Y. Hayashi, H. Arii, Y. Funahashi, T. Ozawa, H. Masuda, Chem. Commun. (2008) 392–394.
[29] H. Carlsson, M. Haukka, A. Bousseksou, J.-M. Latour, E. Nordlander, Inorg. Chem. 43 (2004) 8252–8262.
[30] G.-C. Sun, Z.-H. He, Z.-J. Li, X.-D. Yuan, Z.-J. Yang, G.-X. Wang, L.-F. Wang, C.-R. Liu, Molecules 6 (2001) 1001–1005.
[31] M. Woods, A.D. Sherry, Inorg. Chem. 42 (2003) 4401–4408.
[32] H.S. Soo, A.C. Komor, A.T. Iavarone, C.J. Chang, Inorg. Chem. 48 (2009) 10024–10035.
[33] S. Goswami, N.K. Das, D. Sen, F. Hoong-Kun, Supramol. Chem. 22 (2010) 532–543.
[34] J.A. Drewry, S. Fletcher, H. Hassan, P.T. Gunning, Org. Biomol. Chem. 7 (2009) 5074–5077.
[35] C.A. Bunton, S.J. Farber, J. Org. Chem. 34 (1969) 767–772.
[36] G. Rawji, R.M. Milburn, J. Org. Chem. 46 (1981) 1205–1206.

Please cite this article as: S. Bosch, et al., Asymmetric mono- and dinuclear GaIII and ZnII complexes as models for purple acid phosphatases, J. Inorg. Biochem. (2016), http://dx.doi.org/10.1016/j.jinorgbio.2015.12.028